NUREG/CR-5732
ORNL/TM-11861

Iodine Chemical Forms in LWR Severe Accidents

Final Report

Prepared by
E. C. Beahm, C. F. Weber, T. S. Kress, G. W. Parker

Oak Ridge National Laboratory

Prepared for
U.S. Nuclear Regulatory Commission

AVAILABILITY NOTICE

Availability of Reference Materials Cited in NRC Publications

Most documents cited in NRC publications will be available from one of the following sources:

1. The NRC Public Document Room, 2120 L Street, NW., Lower Level, Washington, DC 20555

2. The Superintendent of Documents, U.S. Government Printing Office, P.O. Box 37082, Washington, DC 20013-7082

3. The National Technical Information Service, Springfield, VA 22161

Although the listing that follows represents the majority of documents cited in NRC publications, it is not intended to be exhaustive.

Referenced documents available for inspection and copying for a fee from the NRC Public Document Room include NRC correspondence and internal NRC memoranda; NRC bulletins, circulars, information notices, inspection and investigation notices; licensee event reports; vendor reports and correspondence; Commission papers; and applicant and licensee documents and correspondence.

The following documents in the NUREG series are available for purchase from the GPO Sales Program: formal NRC staff and contractor reports, NRC-sponsored conference proceedings, international agreement reports, grant publications, and NRC booklets and brochures. Also available are regulatory guides, NRC regulations in the *Code of Federal Regulations*, and *Nuclear Regulatory Commission Issuances*.

Documents available from the National Technical Information Service include NUREG-series reports and technical reports prepared by other Federal agencies and reports prepared by the Atomic Energy Commission, forerunner agency to the Nuclear Regulatory Commission.

Documents available from public and special technical libraries include all open literature items, such as books, journal articles, and transactions. *Federal Register* notices, Federal and State legislation, and congressional reports can usually be obtained from these libraries.

Documents such as theses, dissertations, foreign reports and translations, and non-NRC conference proceedings are available for purchase from the organization sponsoring the publication cited.

Single copies of NRC draft reports are available free, to the extent of supply, upon written request to the Office of Administration, Distribution and Mail Services Section, U.S. Nuclear Regulatory Commission, Washington, DC 20555.

Copies of industry codes and standards used in a substantive manner in the NRC regulatory process are maintained at the NRC Library, 7920 Norfolk Avenue, Bethesda, Maryland, for use by the public. Codes and standards are usually copyrighted and may be purchased from the originating organization or, if they are American National Standards, from the American National Standards Institute, 1430 Broadway, New York, NY 10018.

NUREG/CR-5732
ORNL/TM-11861
R3

Iodine Chemical Forms in LWR Severe Accidents

Final Report

Manuscript Completed: January 1992
Date Published: April 1992

Prepared by
E. C. Beahm, C. F. Weber, T. S. Kress, G. W. Parker

Oak Ridge National Laboratory
Operated by Martin Marietta Energy Systems, Inc.

Oak Ridge National Laboratory
Oak Ridge, TN 37831-6285

Prepared for
Division of Systems Research
Office of Nuclear Regulatory Research
U.S. Nuclear Regulatory Commission
Washington, DC 20555
NRC FIN B0854
Under Contract No. DE-AC05-84OR21400

Abstract

Calculated data from seven severe accident sequences in light water reactor plants were used to assess the chemical forms of iodine in containment. In most of the calculations for the seven sequences, iodine entering containment from the reactor coolant system was almost entirely in the form of CsI with very small contributions of I or HI. The largest fraction of iodine in forms other than CsI was a total of 3.2% as I plus HI. Within the containment, the CsI will deposit onto walls and other surfaces, as well as in water pools, largely in the form of iodide (I^-). The radiation-induced conversion of I^- in water pools into I_2 is strongly dependent on pH. In systems where the pH was controlled above 7, little additional elemental iodine would be produced in the containment atmosphere. When the pH falls below 7, however, it may be assumed that it is not being controlled and large fractions of iodine as I_2 within the containment atmosphere may be produced.

Contents

Appendixes

Figures

Tables

Executive Summary

The analyses in this study were based on quantitative (calculated) results of seven severe accident sequences for light water reactor (LWR) nuclear power plants. These sequences represent a wide range of conditions that are significant risks. Both high- and low-pressure sequences were chosen for three principal plant types; a single sequence was considered for the PWR ice condenser. Each sequence was evaluated by the Source Term Code Package (STCP), and the thermal hydraulics has been documented in previous NRC reports.[1,2] The issue that has been addressed is the chemical forms of iodine in the reactor coolant system (RCS) and in containment — not the ultimate disposition of these chemical forms.

In an LWR accident sequence, fission products released from the core will undergo changes in temperature and concentration as they pass through regions of the RCS. A chemical kinetic model used 20 reactions to determine the control volume where an equilibrium of the iodine, cesium, hydrogen, and steam species becomes "frozen." This means that the temperatures and concentrations of species in subsequent control volumes are not sufficient to reach an equilibrium in the mean residence time available. The "frozen" equilibrium is the species distribution entering containment. Separate equilibrium calculations were performed, using the FACT system,[3] to obtain the distribution of iodine species. The FACT system was chosen in this study because it can be used by anyone who wishes to examine the calculations and its data base contains only assessed data.

In six of the seven calculations, iodine entering the containment from the RCS was almost entirely in the form of CsI; the contributions of I or HI were <0.1% of the overall percentage of iodine.

During the second half of the Surry AB sequence, there is a period during which temperatures in the core region are predicted to be in excess of 2000 K (3141°F) and subsequent volumes of the upper grid plates and guide tubes are at temperatures of only ~500 K (441°F). Under such conditions, the equilibrium compositions in the core region would be "frozen" by the rapid decrease in temperature. For this sequence, the overall iodine distribution was 2.8% as I, 0.4% as HI, with the remainder as CsI. Thus, a total of 3.2% as I plus HI was the largest fraction of iodine in a form other than CsI calculated to enter containment from the RCS in this study.

Once within the containment, CsI is expected to deposit onto interior surfaces and dissolve in water pools, forming iodide (I^-) in solution. The dissolution of HI and HNO_3 (produced by irradiation of N_2 in the atmosphere) and the hydrolysis of I_2 tend to acidify films and pools of water.

Iodine behavior in containment was evaluated during the early stage of an accident sequence, up to ~1200 min. If pH is controlled in containment water pools so that it stays above 7, a reasonable value for the fraction of I^- converted to I_2 is 3×10^{-4}. This yields a small production of volatiles for PWRs, but virtually none for BWRs. Thus, if pH is maintained at 7 or above, only a small additional amount of I_2 is indicated to enter the gas phase in PWR systems.

If the pH drops below 7 (assumed uncontrolled pH), a larger fraction of aqueous I^- will be converted to I_2. Evaporation of this volatile species so as to maintain equilibrium partitioning will result in greater atmospheric I_2, which, in turn, will yield higher organic iodide concentrations. As expected, the levels of airborne iodine volatiles are much higher than in the pH-controlled case, indicating almost complete conversion for PWRs.

The gaseous I_2 fraction is considerably higher in PWRs than in BWRs because of the large water volumes in the latter, which both lower the dose rate and retain greater quantities of dissolved I_2.

In addition, organic iodide is present in PWRs at about 0.5% of core inventory; in BWRs, this value is closer to 0.1%. The I_2 generated by the radiolytic conversion of I^- in containment pools dominates the amount released directly from the RCS as I_2. In addition, due to the equilibrium assumption, the presence of some I_2 already airborne will result in less evaporation of I_2 formed radiolytically. Hence, for the case of uncontrolled pH, the cumulative total

is well represented by the equilibrium amount formed within containment.

The production of I_2 in containment will be directly related to the pH levels of the water pools. There is a significant difference in the amount of I_2 between the uncontrolled-pH and the controlled-pH cases. A major uncertainty in fixing the production of volatile iodine chemical forms in containment involves the extent of evaporation to dryness. At a minimum, 2 to 20% of the iodine in water pools that have evaporated would have been converted to a volatile form, most likely as I_2.

Acknowledgments

The authors acknowledge the aid of Michael Brown, of Thurso, Scotland, who wrote the routine used with the FACSIMILE code and performed scoping calculations for this study. We also wish to express gratitude to Betty Drake for preparing the manuscript. In addition, we appreciate the assistance of Vladimir Kogan of Battelle Columbus Laboratories in obtaining data on accident sequences.

1 Introduction

In the past 10 years, studies of iodine behavior in containment under accident conditions have identified a variety of chemical and physical interactions that will determine the forms of iodine and environments where reactions may occur.[4-7] In general terms, the ability to predict iodine behavior is now more limited by knowledge of the environment in which the iodine is present than by deficiencies in understanding what iodine will do in a given set of environments. Thus, with only a few exceptions, the prediction of chemical form or magnitude of iodine released from containment is limited by the lack of information on the materials and environments involved in iodine reactions in the containment, as well as by uncertainty in the chemical forms and amounts of iodine that enter the containment. For example, it has been found that boric acid and borates are important in determining the chemical forms of iodine in the RCS and in the containment. However, the location, amounts, and type of borate are not well defined in severe accident sequences. A number of tests were performed to examine organic iodide formation with a variety of materials. However, it is not known what organic material will be present and in what form it will exist for a given reactor plant and accident sequence.

Some information on iodine reactions has not yet been put into models and implemented in computer codes. The disparity between information on reactions and models for a computer code is best illustrated by the effect of water radiolysis on iodine chemical forms. Experimental data show that radiolysis can control the chemical forms of iodine in water. Models were developed to calculate water radiation dose rates and pH in severe accident sequences. Modeling of iodine radiolysis at a pH and dose rate in terms of individual reaction rate constants has proven to be extremely difficult because it requires expressions for (1) radiolysis of water, (2) iodine hydrolysis, and (3) the interaction of iodine species with water radiolysis products.

In summary, uncertainties in iodine chemical forms in containment stem principally from uncertainties in the (1) chemical forms and amounts of iodine that enter containment, (2) conditions and materials in which iodine interacts, and (3) lag between obtaining data and implementing it in computer models and codes.

Regulatory Guides 1.3[8] and 1.4[9] state the following:

(1) Fifty percent of the maximum iodine inventory of the reactor core is released to the primary reactor containment; 25% is available for leakage.

(2) Of this 25%, 91% is in the form of elemental iodine, 5% is in the form of particulate iodine, and 4% is in the form of organic iodide.

Iodine is assumed to enter containment in the forms and amounts stated above with neither physical nor chemical changes occurring in containment. However, present knowledge may not support this distribution of iodine forms and the static state throughout the duration of an accident.

It is anticipated that a more "realistic" representation of the chemical speciation of fission product iodine would likely have the following characteristics:

(1) an initial release of some combination of particulate iodine (CsI) and gaseous iodine (HI) or (I), with the largest proportion being particulates

(2) a continuous re-release of molecular iodine that would arise from "revolatilization" from water repositories and would include some small complement of organic iodine

Table 1.1 lists the seven calculated LWR severe accident sequences considered in this analysis; these sequences involve a wide range of conditions that represent significant risks. Both high- and low-pressure sequences were chosen for three principal plant types; a single sequence was considered for the PWR ice condenser. Each sequence was evaluated by the STCP and has been documented in previous NRC reports.[1,2]

Table 1.1 LWR accident sequences evaluated

Plant	Reactor type	Accident	Accident type	Documentation*
Grand Gulf	BWR — Mark III	TC (ATWS)	High pressure	BMI-2104, Vol. III
		TQUV (No makeup water)	Low pressure	BMI-2104, Vol. III
Peach Bottom	BWR — Mark I	TC2 (ATWS)	High pressure	NUREG-4624, Vol. I
		AE (LOCA, no ECCS)	Low pressure	BMI-2104, Vol. II
Sequoyah	PWR — ice condenser	TBA	Low pressure	NUREG-4624, Vol. II
Surry	PWR — large containment	TMLB' (Station blackout)	High pressure	BMI-2104, Vol V
		AB (LOCA, no ECCS) (Station blackout)	Low pressure	BMI-2104, Vol. V

*See References 1 and 2 for complete reference description.

2 Chemical Forms of Iodine Entering Containment from the Reactor Coolant System

2.1 Background

The chemical forms of iodine in the RCS are closely tied to the chemical forms of cesium. The relationship between cesium and iodine in the RCS can be illustrated by the following reaction

$$CsI + H_2O \rightleftharpoons CsOH + HI \qquad (1)$$

The reaction of cesium iodide (CsI) with steam (H_2O), as shown in Equation 1, is the reverse of an acid-base reaction and, thus, is unlikely to proceed unless one or both products are removed. Reactions of CsOH, which tend to lower the partial pressure of CsOH, shift the equilibrium to the right and enhance the formation of HI.

At temperatures in excess of 1800 K (2781°F) and at low hydrogen pressures, iodine as I, rather than HI, is the favored product of the reaction between CsI and H_2O

$$CsI + H_2O \rightleftharpoons CsOH + I + \frac{1}{2}H_2 \qquad (2)$$

Thus, iodine chemical forms other than CsI are favored when steam pressures are much greater than cesium hydroxide pressures.

Fission products released from the core will undergo changes in temperature and concentration as they pass through regions of the RCS. A chemical kinetic model used 20 reactions to determine the control volume where an equilibrium of the iodine, cesium, hydrogen, and steam species becomes "frozen." This means that the temperatures and concentrations of species in subsequent control volumes are not sufficient to reach an equilibrium in the mean residence time available. Separate equilibrium calculations were run, using the FACT system,[3] to obtain the distribution of iodine species. The FACT system was chosen for this study because it can be used by anyone who wishes to examine the calculations and its data base contains only assessed information.

2.2 Data Manipulation and Calculational Techniques

2.2.1 Adaptation of Data from Source Term Code Package

In order to evaluate the chemistry in the RCS, it is necessary to specify the thermal-hydraulic conditions under which reactions would occur. This has been undertaken for each of the accident sequences in Table 1.1 using data from the STCP calculations. Where possible, detailed transient data were taken from the original computer output; otherwise, values were derived from tables or estimated from graphs in the sequence documentation.[1,2] A listing of all the data used is contained in Appendix A.

The chemical equilibrium is calculated in each relevant RCS control volume for the individual sequences. This requires a description of the thermodynamic conditions that occur during various phases of accident progression and a measure of the time span over which such conditions hold.

The MARCH2[10] code generates a special output file that provides input for the TRAP-MELT[11] code. This file was used to identify time-varying values of temperature and pressure in the RCS. Each control volume in the RCS remains constant, and the values used are given in Appendix A. Figure 2.1 illustrates the temperature history of the first two control volumes above core in the Surry TMLB′ accident sequence, where time 0 is at the start of core melting. The figure shows phases of constant or slowly changing behavior in addition to periods of large swings in magnitude. Other sequences exhibit similar patterns.

In addition to T, P, and V, chemical equilibria are dependent on the molar inventories n_i of constituent species H_2, H_2O, I, and Cs. These inventories also vary during the transient and must be obtained for each control volume. Such quantities are calculated

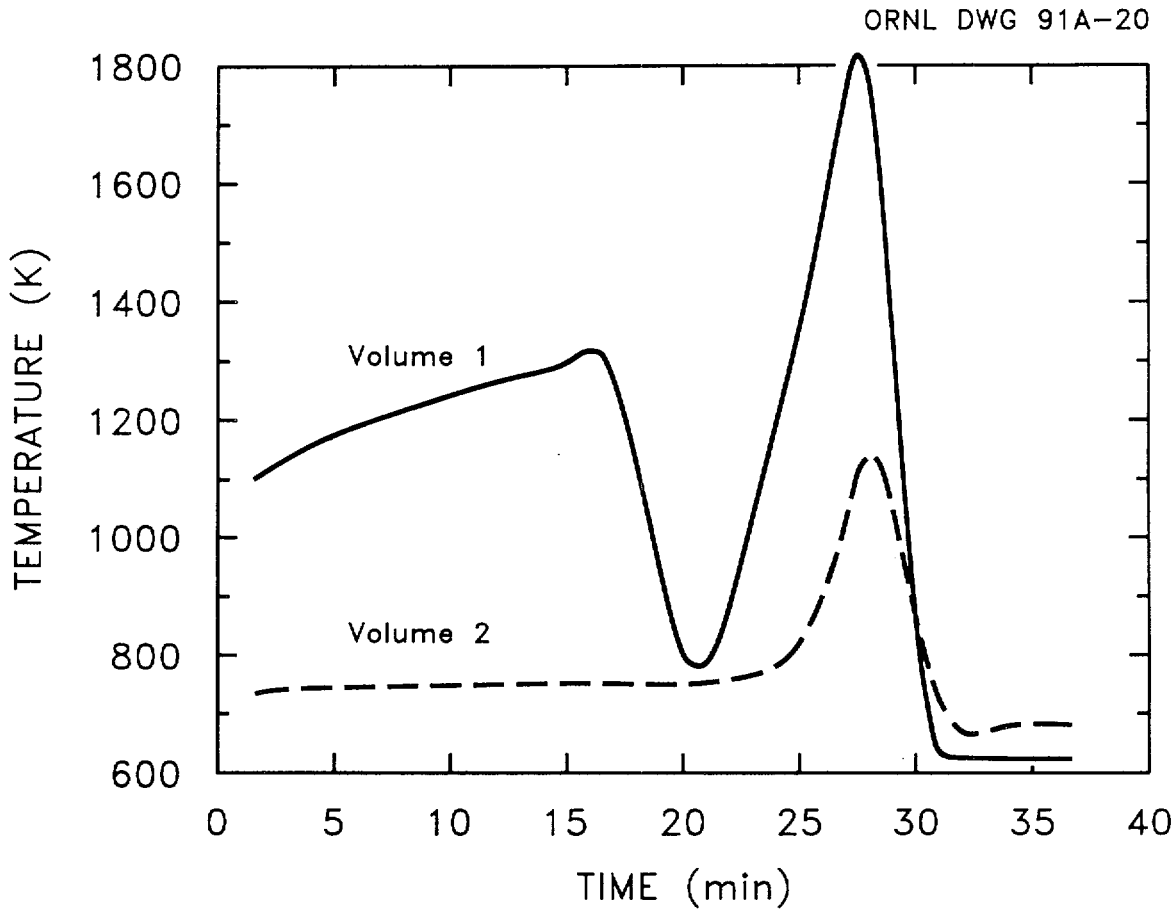

Figure 2.1 Surry TMLB′: temperatures in volumes above core

since they are not directly available from STCP results. Mass flows of H_2 and H_2O and release rates of CsI and CsOH from the core are converted into molar flows (g_{i0}, i = 1, 2, 3, 4) of H_2, H_2O, I, and Cs. These are assumed to directly enter the first control volume above the core. A simple schematic of the system of above-core control volumes is shown in Figure 2.2. Known data are given in normal type, and quantities to be calculated are shown in italics. Although only two control volumes are shown, additional ones could be added (and were for most of the sequences in this study); treatment would be analogous to the second volume in the figure.

Within each control volume, temperature and pressure are assumed to be uniform spatially and constant over computational time intervals (time intervals must be specified small enough to make this valid). From the ideal gas law, the total molar inventory must then also be constant since $n = PV/RT$. This implies that the molar flow (g-mol/s) into a control volume must equal the molar flow out

$$\sum g_{i1} = \sum g_{i2} = \sum g_{i0} = g \qquad (3)$$

Since the inlet flows g_{i0} are known (cf. Figure 2.2), the total flow g can be easily obtained. The volumetric flow v_j from control volume j (m^3/s) is, then

$$v_j = g \frac{RT_j}{P} \qquad (4)$$

and the volume fractional flow from volume j (s^{-1}) is

$$f_j = \frac{v_j}{V_j} = g \frac{RT_j}{PV_j} \qquad (5)$$

Assuming well-mixed control volumes, the flow (mol/s) of constituent i from volume j is represented by

$$g_{ij} = f_i \, n_{ij} \qquad (6)$$

where the molar inventories n_{ij} are updated at each time step by a simple balance equation

$$n_{ij}^{new} = n_{ij}^{old} + \Delta t \, (g_{ij-1} - g_{ij}) \qquad (7)$$

Using this procedure, molar inventories were calculated in each control volume downstream from the core, as were the molar concentrations $C_{ij} = n_{ij}/V_j$. As an example, Figure 2.3 shows the time variation of principal species concentrations for the first control volume above core in the Surry TMLB′ sequence. These concentrations, together with temperature and pressure values, were subsequently used to estimate the equilibrium distributions of chemical species, as described in Section 2.3.1. It is important to note that the equilibrium chemistry was completely decoupled from the mass transfer processes (i.e., no chemical reactions were considered in the flow calculations).

The mean residence time (s) for flow through a control volume is simply the inverse of the fractional flow

$$\tau_j = \frac{1}{f_j} \qquad (8)$$

Figure 2.4 shows this quantity for each of the two control volumes above core in the Surry TMLB′ sequence. As described in Section 2.3.1, a mean residence time >1 s is usually sufficient to attain equilibrium for regions with a sufficiently high temperature. The mean residence time is greater than 1 s for both volumes, although control volume 1 approaches this limit briefly at about 30 min.

The simplicity of this method introduces some uncertainty into the results. However, this uncertainty is generally far less than that due to the input data itself. The time steps were chosen small enough to reduce calculational error to relative insignificance when compared with other sources of error; hence, the chemical reactions may have a slight effect on pressure and temperature, but this is not expected to be significant in altering the inventory and flow patterns. Thus, the results provide a reasonable picture of the chemical thermodynamic conditions in each control volume as the transients progress.

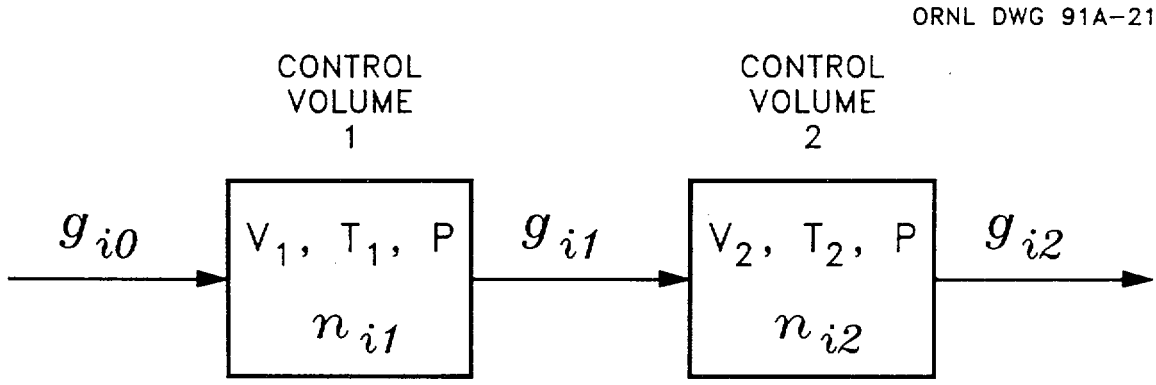

Figure 2.2 **Flow chart of RCS control volumes and variables. Normal type = known data from STCP calculations; italics = quantities to be calculated**

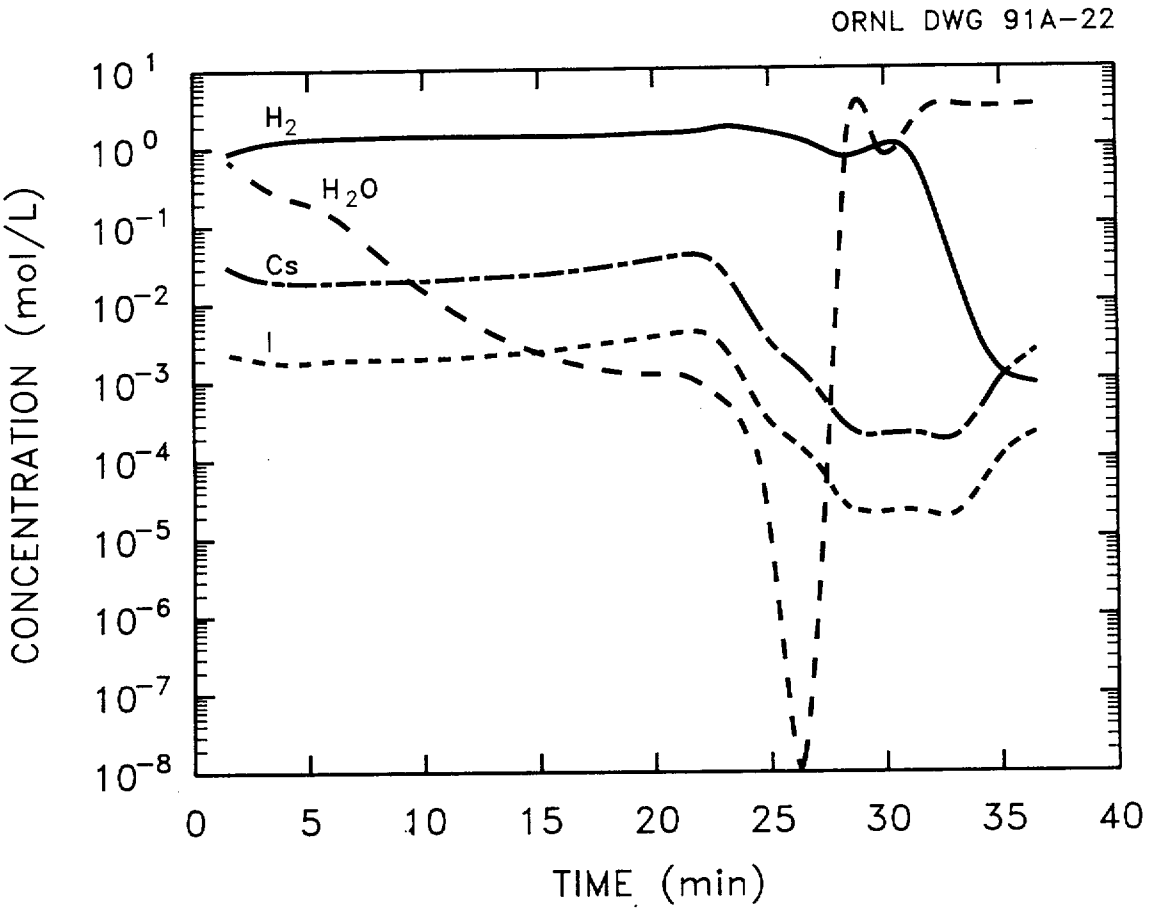

Figure 2.3 Surry TMLB′: principal species concentrations in Volume 1 above core

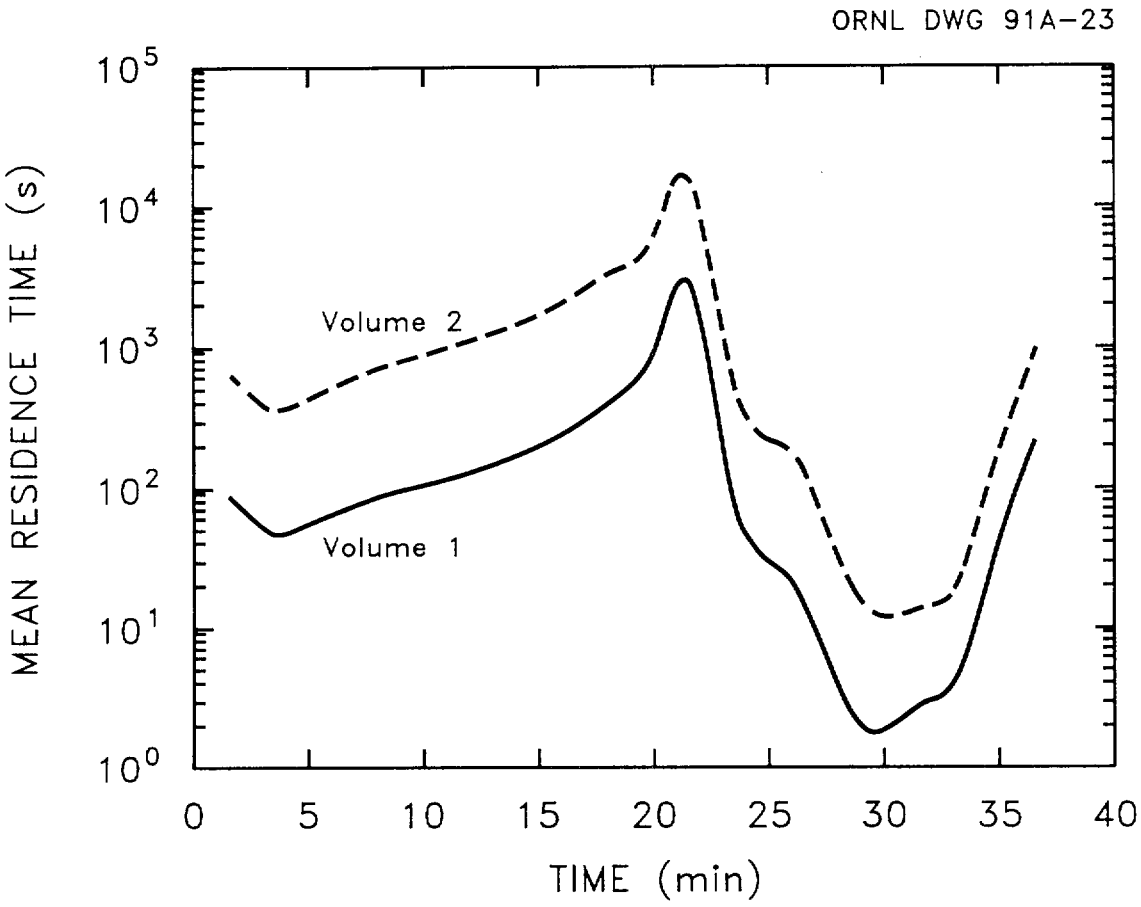

Figure 2.4 Mean residence times in volumes above core for Surry TMLB'

2.3 Iodine-Cesium-Steam-Hydrogen Reactions

2.3.1 Sample Calculations

Kinetic and equilibrium calculations were carried out at frequent intervals during the seven accident sequences. The use of these procedures can be illustrated with the Grand Gulf TQUV sequence at 8780 s. Temperatures of the control volumes are shown in Table 2.1. Kinetic calculations, using the FACSIMILE[12] code, indicated that the equilibrium was not attained in the upper annulus at 907 K (1173°F). However, equilibrium was rapidly attained in the higher-temperature regions. The results of the equilibrium calculations are given in Table 2.1. In the core region, some I and HI were indicated along with CsI. The predominance of I over HI here is the result of reaction 2 being dominant over reaction 1 at the relatively high temperature of this region. Very little I or HI was indicated in the steam separator volume, and essentially only CsI was present in the steam dryers. In this example, the equilibrium was "frozen" at 1180 K (1665°F) in the steam dryer volume because this is the lowest temperature where equilibrium could be attained. If the equilibrium had "frozen" in the core region by quenching from its high temperature without changing composition, then the distribution of iodine species would have been different (see Table 2.1). Calculational techniques used in the seven accident sequences are discussed in Appendix B.

Table 2.1 FACT system output of Grand Gulf TQUV example at 8780 s

Control volumes	Percent CsI	Percent I	Percent HI	Temperature (K)	Temperature (°F)
Core region	91.0	7.5	1.5	2047	3225
Steam separators	99.96	0.01	0.03	1398	2057
Steam dryers	~100.0	<0.01	<0.01	1180	1665
Upper annulus	Not at equilibrium			907	1173

2.3.2 Overall Results of Calculations

In six of seven calculations, the iodine was almost entirely in the form of CsI; the contribution of I or HI was <0.1% of the overall percentage of iodine.

During the second half of the Surry AB sequence, there is a period during which temperatures in the core region are in excess of 2000 K (3141°F) and subsequent volumes of the upper grid plates and guide tubes are at temperatures of only ~500 K (441°F). Because of this, equilibrium compositions in the core region would be "frozen" in by the rapid decrease in temperature. For this sequence, the overall iodine distribution was 2.8% as I and 0.4% as HI, with the remainder as CsI. Thus, a total of 3.2% as I plus HI was the largest fraction of iodine in a form other than CsI in this study.

These calculations considered only reactions involving cesium, iodine, hydrogen, and species, as shown in Appendix B, but covered a wide range of temperatures, hydrogen concentrations, steam concentrations, and fission product concentrations. However, deposition on surfaces and reactions with surfaces were not included in these calculations. Very few specific experimental data about surface

interactions of fission products are available. The effect of these interactions on iodine chemical forms must be carried out with scoping or bounding calculations rather than detailed sequence specific evaluations that were performed for the reactions of iodine and cesium species with steam and hydrogen.

2.4 Reaction of CsOH with Surfaces

2.4.1 Deposition of CsOH onto Structural Surfaces

Of the possible reactions of CsOH in the RCS, the reaction with structural surfaces is the most amenable to evaluation. Johnson et al.[13] have studied the deposition of CsOH on oxidized stainless steel surfaces. They used the following simple expression to relate the thermodynamic activity of CsOH to the surface concentration

$$a = 0.5 \exp\left\{\left(98.5 - \frac{3.84 \times 10^4}{T}\right)(x - 0.28)\right\} \qquad (9)$$
$$x < 0.28$$

where a and x are the surface activity (atm) and concentration (mg/cm^2), respectively. The reaction of interest with stainless steel may be written as

$$\text{CsOH (surface)} \rightleftharpoons \text{CsOH (gas)} \qquad (10)$$

Thermochemical data obtained from the FACT system[3] give the respective equilibrium constants for the reactions in Equations 1 and 9 as

$$K_1 = \frac{P_{CsOH}}{P_{H_2O}} \frac{P_{HI}}{P_{CsI}} = \exp\left(-1.407 - \frac{1.626 \times 10^4}{T}\right) \qquad (11)$$

$$K_9 = \frac{P_{CsOH}}{a} = \exp\left\{1.189 \times 10^1 - \frac{1.500 \times 10^4}{T}\right\} \qquad (12)$$
$$900 \le T \le 1263$$

Calculations using Equations 9, 11, and 12, together with mass balances on cesium and iodine, indicate that the amount of HI formed due to the CsOH surface reaction is less than 0.6% for each of the accident sequences studied. This is because P_{CsOH} must be very small if the ratio P_{HI}/P_{CsI} is large enough to be significant. However, if P_{CsOH} is very small, then so is x; hence, very little surface reaction could occur.

2.4.2 Other Reactions of CsOH

Other reactions of CsOH may also remove it from the vapor phase, but there is generally a lack of information on the amounts and locations of other reactants. For example, several cesium borates may form in the reaction of CsOH with boric acid or boron oxide. The formation of cesium metaborate ($CsBO_2$) may occur by the following reaction

$$CsOH + HBO_2 \rightleftharpoons CsBO_2 + H_2O \qquad (13)$$

At equilibrium at 1000 K (1341°F), the pressure of CsOH may be written as

$$P_{CsOH} = \sim 1.6 \times 10^{-11} \cdot \frac{P_{H_2O}}{P_{HBO_2}} \qquad (14)$$

If sufficient meta-boric acid (HBO_2) were available, it could result in a lowering of the vapor pressure of CsOH.

Two simulated core-melt tests were run at ORNL to assess boric acid volatility and the potential for vapor interactions with CsI. Two different sized simulant fuel bundles were used—nominally 1 and 10 kg. The smaller, 1-kg, fuel simulant bundle consisted of 12 zirconium tubes (10.16 cm long) with 0.247 kg end caps, 0.093 kg stainless steel grids, 0.0185 kg Inconel grids, and 0.585 kg UO_2 pellets. There were no added Cs or I species in the small bundle test. The test was performed by inductively heating the fuel bundle while injecting feedwater containing 2000 ppm boric acid into the bottom of the bundle. In this test, it was found (see Table 2.2) that during the lower-temperature heating steps up to 1600°C, ~10% of the boron was transported through the bundle and was captured downstream as boron oxide. As the temperature was increased to partial melting of the bundle, the collected B_2O_3 decreased. This decrease was

Table 2.2 Simulated core-melt tests conducted in the ORNL 1-kg facility (Boric acid addition to water injected below the bundle)

Heating step	Total boron present* (g)	Boron collected as B_2O_3	
		Filter (%)	Wash (%)
A (1600°C)	0.034	10.37	0.0
B (1800°C)	0.088	5.5	0.68
C (2400°C)	0.142	0.024	0.009

*As boric acid in water used for steam generation.

attributed to increased reactivity of the boron oxide with the hot fuel and clad oxides.

The composition of the 10-kg fuel bundle is shown in Table 2.3. Note that in this test, CsI was added to 12 of the 60 simulant fuel rods in a limited region near the bundle centerline. Excess cesium was not added.

The 10-kg test was conducted at a bundle centerline temperature limit of 1600°C, which was reached in ~30 min and maintained for an additional 30 min. During this time, 365 mL of boric acid solution containing 3.83 g of H_3BO_3 was added to the steam generator porous media below the fuel bundle. Hydrogen release measured 326 L, which would be equivalent to 72% conversion of the water and ~30% reaction of the Zircaloy in the bundle.

Analytical results from X-ray diffraction showed that white solids observed plated out on the quartz chimney were nearly pure CsI with no detectable B_2O_3. Chemical analysis of the washings from the system indicated that nearly half of the CsI had vaporized and that no boron-containing materials were present. This complete failure to find any B_2O_3 downstream of the bundle was somewhat unexpected since the 1-kg test had resulted in some penetration of boron oxide. It is likely that the extra length of the 10-kg system prevented penetration by the reaction of B_2O_3 with ZrO_2. A sample analysis of a white oxide (a thin ring of mixed ZrO_2 and B_2O_3) in a very highly refractory solid solution on the oxidized clad surface was estimated to account for about one-third of the total boron added. The remainder of the boron oxide appeared to be associated with the porous ZrO_2 steam generator base at the bottom of the bundle. A test scrubber that had been operated continuously on a diverted part of the hydrogen/steam flow showed no evidence of volatile (nonparticulate) iodine.

Similar results were subsequently obtained in a test with silver vaporized in a 10-kg bundle containing Ag-In-Cd alloy control rod simulants. In the latter case, cadmium vapor was observed downstream, but the silver did not penetrate out of the bundle—presumably because of interactions with Zircaloy.

Based on these results, it is highly likely that boric acid covaporized from residual water below the core in severe accidents will be tied up by the Zircaloy in the lower regions of the core and will not be available airborne to affect the chemical form of the released iodine.

2.5 Revaporization of CsI from RCS Surfaces

2.5.1 Description of Revaporization Process

During an accident sequence, CsI may condense on RCS surfaces. If the temperature increases later in the sequence, the CsI may revaporize into a gas with very little cesium hydroxide. The revaporization of CsI can be expressed as

Chemical Forms

Table 2.3 Composition of 10-kg fuel bundle

Item	Weight* (g)
60** — Zircaloy tubes	2181.0
120 — Zircaloy end caps	503.6
3 — Stainless steel grids	342.0
1 — Inconel grid	112.0
4 — Stainless steel supports and screws	58.5
2 — Stainless steel lifts and screws	9.0
UO_2 pellets	(N.W.) 7464.0 (E.W.) 6739.9
UO_2 powder	(N.W.) 1201.9 (E.W.) 1059.5
$SrCO_3$	3.00
$BaCO_3$	4.05
La_2O_3	2.28
Eu_2O_3	0.21
Sm_2O_3	1.12
CeO_2	4.87
Mo	4.70
Te	0.82
Ru	5.16
CsI†	0.85

*N.W. = net weight; E.W. = uranium element weight.
**Twelve of these tubes had three horizontal slits each, 0.010 in. wide × 1 in. long, and 120° apart in their midsection.
†CsI mixed with 300 g UO_2, rare earths, and metal powders was added to the ~1-in. section of the 12 tubes.

$$CsI\ (liquid) \rightleftharpoons CsI\ (gas) \qquad (15)$$

The vapor pressure of CsI, calculated with data obtained from the FACT system,[3] is

$$P_{CsI} = \exp\left[\frac{-2.021 \times 10^4}{T} + 1.307 \times 10^1\right] \qquad (16)$$
$$T = 1000 - 1553\ K$$

In Equation 1, a mole of CsOH would be produced for every mole of HI. Assuming that this is the only CsOH (gas) in the system for the sake of a bounding calculation, the equilibrium constant for reaction 1 may be arranged as

$$P_{HI}^2 = P_{CsI} \cdot P_{H_2O} \exp\left\{-\left(\frac{1.622 \times 10^4}{T} + 1.467\right)\right\} \qquad (17)$$
$$T = 1000 - 1553\ K$$

2.5.2 Assessment of Revaporization as a Source of HI

From Equation 17, P_{HI} may be calculated if P_{H_2O} is known or assumed and P_{CsI} is calculated from Equation 16. The calculated percentages of iodine as HI when P_{H_2O} = 1 atm varied from 0.5% at 1000 K to 0.25% at 1553 K. At higher steam pressures, proportionately higher percentages as HI may occur.

To assess an upper bound on the extent of HI formation by revaporization of CsI, the following assumptions are made:

(1) The temperature of revaporization is the temperature where equilibrium was "frozen."

(2) The steam pressures are those obtained from the seven accident sequences.

(3) The only CsOH (gas) in the system is that produced by Equation 1 and is, mole for mole, the same as HI. All other cesium was somehow removed (i.e., vented).

(4) All of the iodine deposited on the surface and was subject to revaporization as described by Equations 15 and 16.

Table 2.4 indicates the estimated upper bounds on the fraction of iodine as HI that results from these assumptions. The highest percentages as HI were obtained from those accidents in which steam pressures were >1 atm for a significant time during the sequence. These upper bounds probably overestimate the formation of HI in several ways:

(1) It is not likely that all iodine would deposit as CsI and be subject to later revaporization.

(2) The steam pressures used in the calculations were those of the accident sequences. Revaporization could occur after steam pressures had decreased.

(3) The cesium hydroxide pressure would most likely be greater than the HI pressure. As described in Section 2.4.1, it would be difficult to reduce CsOH pressures low enough to influence HI formation by deposition of cesium on stainless steel.

2.6 Summary of Iodine Chemical Forms in the RCS

Iodine entering containment from the RCS should be predominantly in the form of CsI. The examination of Cs-I-H_2O-H_2 interactions for seven accident sequences gave a maximum of 3.2% iodine as I plus HI, with the remainder as CsI. There are some uncertainties in the reactions of CsOH with oxides, as well as in the revaporization of CsI, that produce uncertainties in the extent to which iodine may exist in a form other than CsI. Cesium needs to be removed from reactions involving iodine if very much iodine is to be in a form other than CsI.

Based on this analysis, the chemical forms of iodine entering containment from the RCS may reasonably be described as a maximum of 5% as elemental iodine and HI, with not less than 1% as either elemental iodine or HI. The remaining 95% would be CsI.

Table 2.4. Estimated upper bound on the fraction of iodine as HI due to revaporization of CsI

Accident sequence	Estimated percentage of iodine as HI*
Grand Gulf TC	0.3
Grand Gulf TQUV	0.4
Peach Bottom AE	0.6
Peach Bottom TC2	3.1
Sequoyah TB	2.4
Surry TMLB'	3.8
Surry AB	0.03

*Note: See Section 2.5.2 for a list of assumptions used in calculating these estimated values.

3 Iodine Behavior in Containment

3.1 Categorization of Iodine Behavior in Terms of Time Intervals During an Accident Sequence

Based on TRENDS models, calculations of iodine behavior for NUREG-0956,[14] and information from large-vessel tests[15-18] as well as from the accident at TMI-2, the iodine behavior may be separated, by time, into three categories: (1) from initial release into containment up to 1000 to 1200 min following initiation of the accident, (2) from 1000 to 1200 min to ~2 to 3 weeks, and (3) for times greater than ~3 weeks.

Category 1. Iodine Behavior. In this time interval, the uncertainty in the amount and chemical forms that enter containment is most important. The upper time limit for this category is the time when airborne aerosol concentrations have been substantially reduced from their peak values. The source term calculations in previous reports[1,2] stopped in the range of 1000 to 1200 min.

All of the chemical and physical interactions of HI are expected to occur during this time interval. Events leading to the formation of I_2 by radiolysis would also occur in this interval and the next time interval as well. Thus, during this period, all material of importance to iodine reactions is expected to deposit in water pools or onto surfaces, all gaseous iodine-aerosol interactions are expected to take place, and all HI effects, except for those related to pH, are expected to occur.

Category 2. Iodine Behavior. In this time interval, vapor-phase iodine will consist of I_2 produced by radiolysis and partitioned between aqueous solution and the gas, as well as organic iodide. Iodine will also be found in aqueous solution in forms that are determined both by radiolysis and by pH and deposited on structural surfaces. In this time interval, the chemical forms of iodine should not be closely related to the chemical forms that entered containment from the RCS because the iodine would have interacted with a surface and/or dissolved in water.

Category 3. Iodine Behavior. At long times after a severe accident, gas-phase iodine is expected to be dominated by organic iodide with a small contribution from I_2. Approximately 15 months following the accident at TMI-2, the concentration of ^{129}I in containment gas was $3.3 \times 10^{-12} \pm 8.9 \times 10^{-13}$ mol I/L.[19] Methyl iodide is an "ubiquitous" halocarbon that is present in the atmosphere at concentrations which vary somewhat with distance from the ocean. In a study of eight locations in the United States, the overall mean concentration was $\sim 2 \times 10^{-12}$ mol CH_3I/L.[20] Thus, the long-term organic iodide concentration in containment will probably be on the order of 10^{-12} mol I/L. Iodine behavior and distribution, in the long term, are expected to have little relationship to the chemical forms or amounts released into containment because the iodine would have had time to deposit on surfaces or in water pools and the environmental conditions in containment would prevail in determining the chemical forms.

3.2 Importance of pH in Determining the Chemical Forms of Iodine in Water Pools

3.2.1 Materials That Determine pH in Accident Sequences

Results of various experiments have shown that solution pH is the major factor in determining the amount of I_2 and organic iodide formation in solution.[4] Materials that can determine pH in containment water pools are given in Table 3.1. This list includes both acidic and basic materials. In situations in which no chemical additives are present to control pH, the amounts of HI, cesium borate or hydroxide, and boron oxides reaching a sump will initially determine pH. In some sequences, the core-concrete interaction would produce aerosols that contain the basic oxides K_2O, Na_2O, and CaO. The influence of these oxides on pH will depend on the amount that has entered the water pool, the initial pH and buffering capacity of the solution, the quantity of

Table 3.1 Materials that affect pH in containment water pools

• Boron oxides (acidic)
• Basic fission product compounds such as cesium hydroxide or cesium borates (basic)
• Iodine as HI (acidic)
• pH additives (basic)
• Atmospheric species such as carbon dioxide or nitric acid (acidic)
• Core-concrete aerosols (basic)
• Pyrolysis and radiolysis products from organic materials (acidic)

water, and the extent of dissolution of the aerosol material. One of the TRENDS models calculates the pH in water pools.

3.2.2 Nitric Acid Formation and pH Control

Water that is exposed to air absorbs CO_2 to form carbonic acid, which lowers pH. The pH of water approaches a limiting value of ~5.65 due to this process. In addition, nitric acid can be produced by the irradiation of water and air. Table 3.2 shows the relationship between the formation of nitrate ions and hydrogen ions from the irradiation of an air-water system. Table 3.3 shows the decrease in pH for an irradiated solution that contained trisodium phosphate with an initial pH of 9.0. During the irradiation, nitric acid and atmospheric CO_2 decreased the pH as shown. Phosphate solutions have their maximum pH buffer capacity at a pH near 7. This buffer capacity is reflected here in the length of time that the pH remained near 6.5. Once the buffer capacity was exceeded, the pH continually decreased.

Because of CO_2 and nitric acid, the pH is not likely to remain at some preadjusted value. A buffer system to retard changes from the desired pH is expected to provide a more stable pH level.

Two different buffer systems could be used in containment water pools: a phosphate buffer and a borate buffer. The phosphate buffer has a maximum capacity near pH 7, while the borate buffer has its maximum capacity near pH 9. Buffer capacity is often evaluated in terms of its buffer value B, which is defined by

$$B \equiv \frac{db}{dpH}$$

where db is an increment of strong base in mol/L. With the addition of strong acids, a negative increment $-db$ is used. Bates[21] has shown that the relationship between the maximum buffer value, B_{max}, and concentration of a buffer, C, can be written as:

$$B_{max} = 0.576\ C$$

Thus, a given concentration of phosphate would have the same buffer value at a pH near 7 that the same concentration of borate would have at a pH near 9. The selection of the buffer system is important in determining the pH to be maintained. From a strictly chemical standpoint, selecting a borate for the buffer to maintain a pH near 9 is just as simple as selecting a phosphate to maintain a pH near 7.

Table 3.2 Concentrations of H^+ and NO_3^- in water due to irradiation*

Irradiation time (h)	$[H^+]$ from pH	$[NO_3^-]$ from ion electrode
6	3.2×10^{-5}	6.5×10^{-5}
12	6.3×10^{-5}	6.7×10^{-5}
22	1.0×10^{-4}	1.0×10^{-4}
65	2.5×10^{-4}	1.8×10^{-4}
114	5.0×10^{-4}	4.0×10^{-4}

*100 mL in closed 200-mL container at rate of 0.6 Mrad/h.

Table 3.3 Effects of irrradiation dose* on pH in trisodium phosphate solution

Time (h)	pH
0	9.0
4	6.4
7	6.5
23	6.5
41	4.7
63	3.9

*Dose rate, 0.53 Mrad/h.

Recently, a patent was issued for a method of pH control and gettering of iodine species which employs well-dispersed silver carbonate.[22]

3.3 Processes That Alter the Chemical Forms of Iodine in Containment

3.3.1 Radiolysis

3.3.1.1 Description of Calculated Model

In the presence of radiation, the equilibrium formation of I_2 from I^- is strongly dependent on pH and weakly on temperature and concentration. Ignoring the last two effects,[4] this dependence can be written as

$$F(pH) = \textit{equilibrium fraction} = \frac{[I_2]}{[I_2] + [I^-]} \qquad (18)$$

where [x] is the concentration of I_2 or I^- (g-atom/L). Data from Lin,[23] as shown in Figure 3.1, illustrate this effect for several initial concentrations and pH values using solutions that were at ambient temperature and had been irradiated for 1 h at 4.5 Mrad/h. The final pH values were not indicated but probably decreased slightly since no mention is made of buffering in the experiment. The values of pH >6 may not be quantitatively useful since the very small conversion fractions are probably incorrect due to measurement error. As seen in Figure 3.1, F is near 0 for pH >7 and near 1 for pH <2 but experiences a drastic change in the

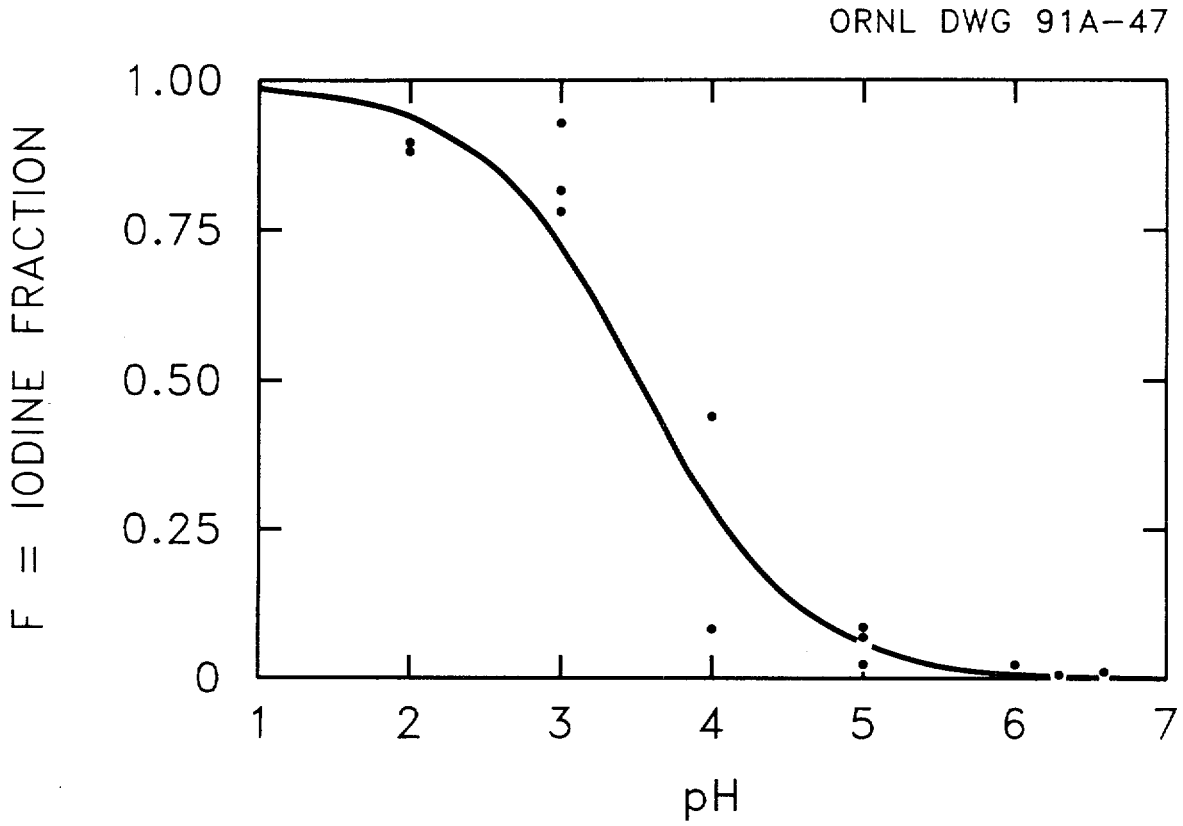

Figure 3.1 Radiolytic conversion of I^- to I_2 [data from C. C. Lin, *J. Inorg. Nucl. Chem.* 42, 1101 (1980)]

range $3 < pH < 4$. As discussed in Appendix C, this can be effectively modeled by the functional form

$$F = [1 + e^{\alpha\ pH + \beta}]^{-1} \qquad (19)$$

Equation 19 was fit to Lin's data by minimizing the sum of least-squares residuals, which yields

$$\alpha = 1.72 \qquad \beta = -6.08 \qquad (20)$$

Similar data are given by Naritami et al.[24] for $5 \le pH \le 9$. They subjected borated I^- solutions of 10^{-4}, 10^{-5}, and 10^{-6} mol/L to much lower dose rates (^{60}Co gamma rays of 0.1 Mrad/h) for 1 h. The model of Equations 19 and 20 gives a good match to these data for concentrations of 10^{-4} mol/L, although the model overestimates conversion for the lower concentrations.

If the pH is maintained sufficiently high through buffering or addition of sufficient basic material, very little conversion will occur. In this case, most iodine remains dissolved as I^-. Lin's data generally indicate <1% conversion at pH = 7. This value declines as the total iodine concentration decreases. The data of Naritomi show a conversion of 0.2% for iodide concentrations of 10^{-4} mol/L and 0.01% at lower concentrations. Data measured for this study indicate that for a dose rate of 0.35 Mrad/h, an iodine concentration of 10^{-4} mol/L conversion was 0.003% after 4 h irradiation and 0.03% after 24 h. The last value, 0.03%, has been used in the present work.

If the pH level is not deliberately controlled, it may decrease sufficiently to allow considerable conversion of I^- to I_2. The primary mechanism is radiolytic generation of nitric acid (see Section 3.2.2). If the pH is neutral initially, then this effect soon dominates, resulting in

$$[H^+] = 10^4\ g(HNO_3)\ \frac{E_{dep}}{V_L N_a} \qquad (21)$$

where

$[H^+]$ = concentration of H^+ (mol/L),
$g(HNO_3)$ = rate of HNO_3 production due to irradiation (molecules/100 eV),
E_{dep} = total energy deposition due to fission product decay (MeV),
V_L = volume of water (L),
N_a = 6.022×10^{23} (molecules/mol).

The data in Table 3.2 indicate that at 30°C (86°F)

$$g(HNO_3) = 0.007\ molecules/100\ eV \qquad (22)$$

This relationship is based on radiation absorption by the aqueous phase. The actual mechanism for the formation of nitric acid is not known. It may occur in the aqueous phase, in the gas phase, or at the gas-surface interface. The containment water volume, V_L, is usually constant over the period during and subsequent to significant fission product releases.

The energy deposition over a time Δt is

$$E_{dep} = \dot{E}_{dep}\ \Delta t = \Delta t \sum m_j\ \dot{e}_j \qquad (23)$$

where

Δt = time (h),
$\dot{E}_{dep}$ = total energy deposition rate (MeV/h),
m_j = mass of nuclide group j in pool (g),
$\dot{e}_j$ = energy deposition rate per unit mass of nuclide group j (MeV/h-g).

Various groupings of fission products and actinides have been considered in past safety studies. A grouping compatible with that used in STCP accident studies was selected for this study (see Table 3.4). The specific energy deposition rate $\dot{e}_j$ for each group depends on the relative distribution of radioactive nuclides, which, in turn, depends on such factors as fuel enrichment, power history, and additives or other materials in the fuel or reactor.

A detailed analysis of Browns Ferry (a large BWR with Mark I containment) accident sequences has been performed by ORNL staff members. Using the ORIGEN2 code,[25] nuclide inventories were determined for the highest and lowest power of each type of fuel

Table 3.4 Nuclide groupings and group-specific energy deposition rates

Group index, j	Characteristic element	Included nuclides	Energy deposition rate, $\dot{e}_j \times 10^{-19}$ (MeV/h·kg)
1	I	I, Br	425.0
2	Cs	Cs, Rb	3.971
3	Te	Te, Se, Sb	20.06
4	Sr	Sr	31.25
5	Ba	Ba	8.900
6	Ru	Ru, Tc, Rh, Mo, Pd	6.613
7	Ce	Ce, Pu, Np	1.540
8	La	La, Am, Cm, Y, Pr, Nd, Pm, Sm, Eu, Zr,* Nb	25.46
9	Xe	Xe, Kr	2.902

*Includes only fission products.

assembly in the cycle 6 fuel loading. Nuclide inventories for every assembly in the reactor were then determined by interpolation based on power history, using the high and low cases for that assembly type. These inventories were subsequently combined to obtain a total core inventory for every fission product nuclide of significance either in mass or decay energy at 5 h after shutdown. Assuming all decay energy is absorbed, the total inventories were used with decay energy data for each nuclide to obtain energy deposition rates e_j for each fission product group, which are also shown in Table 3.4. Complete details of this calculation can be found in Reference 26.

The group energy deposition rates for the Browns Ferry BWR are applied to all sequences considered in the present study. This is a very legitimate assumption for the Peach Bottom plant, which is also a BWR-Mark I nearly identical to Browns Ferry in size and design. A similar assumption is also made for Grand Gulf, also a BWR. These assumptions are analogous to those made in previous reports[1,2] using ORNL calculations for the Browns Ferry cycle 4 loading. While PWRs have many characteristics different from BWRs, the fission process results in the same distribution of fission products. Although the final distribution is somewhat affected by geometry and additives, the group energy deposition rates are assumed to be sufficiently similar to BWR values to permit use of the values in Table 3.4 for Sequoyah and Surry sequences.

3.3.1.2 Mass Manipulations

The group masses m_j are obtained by multiplying the total core inventory $\bar{m}_j$ by the estimated fractional release into containment

$$m_j = f_j \bar{m}_j \qquad (24)$$

Total core inventories for the plants are those identified in previous reports[1,2] and are given in Appendix D. Various estimates of the fractional releases f_j can be obtained from Nourbakhsh.[27] He has compiled results from many STCP accident calculations (including those mentioned in this study) and has stated bounding estimates for the fractions of core inventory released into containment due to the following effects:

(1) release from RCS prior to vessel failure
(2) release at vessel breach
(3) ex-vessel release due primarily to core-concrete interactions

(4) late revolatilization from the RCS.

Categories 1, 2, and 4 can be combined to yield a total release into the containment from the primary system. The release fractions adopted from Nourbakhsh and used in this study are shown in Table D.2 of Appendix D.

Finally, Δt in Equation 23 is the time needed to reach the approximate steady state. In general, the first phase of an accident can be considered to reach steady state in 10 to 15 h (see Section 3.1), and this is the time range considered for Δt. The pH can be calculated from

$$pH = -\log_{10} [H^+] = -\ln [H^+]/\ln 10$$

and the fractional conversion in Equation 18 then takes the form

$$F = \left[1 + e^{b[H^+]^{-\frac{a}{\ln 10}}}\right]^{-1} = \left[1 + 5.55 \times 10^{13} \left(\frac{V_L}{E_{dep}}\right)^{0.747}\right]^{-1} \quad (25)$$

Thus, when pH is not controlled, fractional conversion is directly dependent on the liquid volume V_L in which radiolysis occurs; the energy deposition E_{dep}, which itself depends on the amounts of radioactive species in water; and the time Δt allowed for the radiolysis process to reach steady-state conditions.

3.3.1.3 Gas-Liquid Partitioning

The equilibrium distribution of a single volatile species, such as I_2, is represented by the partition coefficient

$$P = \frac{[I_2\ (aq)]_{eq}}{[I_2\ (g)]_{eq}} \quad (26)$$

This quantity is inversely related to the Henry's Law constant K (i.e., $P = 1/K$) and should not be confused with the overall iodine partition coefficients often used in reactor safety studies. Partition coefficients for I_2 were calculated from

$$\log_{10} P = 6.29 - 0.0149\ T \quad (27)$$
$$T\ (K)$$

This relationship gives the experimental value reported by Eguchi et al.[28] and by Sanemasa et al.[29] at 298 K (77°F). Extrapolation of the experimental results of these investigators to 373 K (212°F) yielded a partition coefficient of 3. Furrer et al.[30] reported a calculated partition coefficient at 373 K (212°F) of 9.

Some of the data used in this calculation was based on estimated parameters. Equation 27 gives a partition coefficient of 5.3 at 373 K (212°F), the approximate average of the calculated value, and the extrapolation of the measured values.

While it may take considerable time to approach such equilibration in a large system such as a reactor containment, Equation 26 can still be used to estimate I_2 volatility. In fact, instant equilibration is a conservative assumption since considerable holdup could be expected in real-life situations. A rigorous analysis would consider the delay associated with the evaporation of volatile species from water pools. This phenomenon is not well understood, and only crude models are available. Thus, the escape of I_2 from water pools will be modeled by assuming that Equation 26 holds continuously as I_2 is produced radiolytically.

3.3.1.4 Gas-Phase Reactions: Formation of Organic Iodides

The process of converting I_2 into organic iodides (chiefly CH_3I) is still not fully understood. Postma and Zavodoski[31] reviewed production rates from about 70 containment tests and determined that the asymptotic steady-state conversion to CH_3I was

$$percent\ I_2\ converted = 0.19\ C_{mo}^{-0.26}, \quad (28)$$

where C_{mo} = initial I_2 concentration (mg/m^3). This equation was based on 69 containment experiments. In a more recent review, Beahm et al.[5] described formation using the rate equation

$$\frac{dC_o}{dt} = \alpha(C^* - C_o) \qquad (29)$$

where

α = formation rate constant (s^{-1}),
C_o = organic iodide concentration (mg iodine/m^3),
C^* = steady-state organic iodide concentration (mg iodine/m^3).

They assigned the constant value $\alpha = 0.0051$ based on empirical evidence and used

$$C^* = 0.0189\ C_{mo}^{0.82} \qquad (30)$$

in place of Equation 28. This equation was based on containment experiments performed with irradiated fuel rather than simulated materials. The percent conversion to organic iodide when irradiated fuel was used was somewhat greater than that obtained from simulant materials (cf. Figure 4, Reference 5).

By converting units to g-atom/L, Equation 30 can be rewritten as

$$[CH_3I] = \beta\ [I_2]^{0.82} \qquad (31)$$

where $\beta = 0.0189\ (10^6 \cdot MW)^{-0.18}$, MW being the molecular weight of I. For MW = 130, then $\beta = 6.55 \times 10^{-4}$, which indicates that generally <1% of gaseous iodine will be organic.

3.3.1.5 Overall Behavior

As described in the previous sections, the distribution of species throughout the gas and liquid phases can be estimated from models for three basic processes: radiolytic conversion of I^- to I_2 in water, evaporation of I_2, and gas-phase formation of organic iodides. Defining the desired quantities as concentration variables (g-atom/L)

$$C_1 = [I_2\ (aq)],\ C_2 = [I_2\ (g)],\ C_3 = [I^-\ (aq)],$$
$$C_4 = [CH_3I\ (g)]$$

Equations 26, 18, and 31 can be rewritten as

$$C_1 = PC_2 \qquad (32a)$$

$$C_3 = \frac{(1 - F)}{F}\ C_1 \qquad (32b)$$

$$C_4 = \beta\ C_2^{0.82} \qquad (32c)$$

In addition, the total iodine inventory N_T (g-atom) is equal to the initial I^- entering the containment and remains constant throughout the distribution process:

$$N_T = V_L\ (C_1 + C_3) + V_g\ (C_2 + C_4) \qquad (32d)$$

There are four equations (Eqs. 32a—32d) and four unknowns (C_1, C_2, C_3, and C_4); all equations except Equation 32c are linear, and its nonlinearities are very mild.

To obtain solutions to the system, Equations 32a—32c are substituted into Equation 32d, yielding

$$N_T = \frac{V_L}{F}\ PC_2 + V_g\ (C_2 + \beta C_2^{0.82}) \qquad (33)$$

which can be arranged into the form

$$C_2 = \frac{\left(N_T - V_g\ \beta C_2^{0.82}\right)}{\left(\frac{PV_L}{F} + V_g\right)} \qquad (34)$$

This represents a convenient form for fixed-point iteration, which usually converges to a relative error of 10^{-4} within three to five iterations. Once C_2 has been determined from Equation 34, the other concentrations are obtained from Equations 32a—32c.

Because organic iodide is such a small part of the total, it is helpful to examine the distribution behavior without considering organic iodide. By ignoring Equation 32c, Equation 33 becomes

$$N_T = \frac{V_L}{F} PC_2 + V_g C_2$$

which can be rearranged to obtain

$$\frac{N_2}{N_T} = \left(1 + \frac{V_L P}{V_g F}\right)^{-1} \qquad (35)$$

where $N_2 = V_g C_2$ = g-atom of I_2 in gas. Equation 35 is a convenient expression of the fraction of iodine that is volatilized. (Consideration of organic iodide will increase this fraction very slightly.) For the case of uncontrolled pH, substitution of Equation 25 into Equation 35 yields

$$\frac{N_2}{N_T} = \left\{1 + \frac{V_L P}{V_g}\left[1 + 5.55 \times 10^{13}\left(\frac{V_L}{E_{dep}}\right)^{0.747}\right]\right\}^{-1} \qquad (36)$$

which is an expression for the fraction of volatile iodine (as I_2). To use Equation 35 or 36, it is necessary to estimate the characteristics or approximate values for each of the following quantities:

V_L, V_g = liquid and gas volumes (L),
T = air-water interface temperature (which permits computation of the partition coefficient P by Equation 27).

For the case of uncontrolled pH, it is also necessary to obtain

m_i = masses of fission products in the containment (from which the dose term E_{dep} is calculated by Equation 24),
Δt = approximate duration of the radiolysis phase(s) in category 1 (see Section 3.1).

If Equation 35 or 36 is used instead of solving the nonlinear Equation 34, then a good approximation to the airborne organic iodide inventory can be obtained by simply using Equation 32c. Furthermore, Equations 35 and 36 are in particularly convenient form not only to estimate iodine volatility, but also to estimate the individual phenomena and their impact on overall behavior.

3.3.2 Results of Iodine Behavior in Containment

The analysis described in Section 3.3.1 has been applied to each of the seven accident sequences listed in Table 1.1. Using whole core inventories from previous reports,[1,2] the release fractions of Nourbakhsh[27] (including both vessel and core-concrete releases), and the nuclide group energy deposition rates in Table 3.4, the energy deposition rate $\dot{E}_{dep}$ can be calculated for each plant using Equations 23 and 24. The results are shown in Appendix E.

Once the energy deposition has been computed, the remaining quantities can be calculated by solving the system of equations 32. Liquid and gas volumes and temperatures were obtained from sequence documentation.[1,2] The gas volumes used for BWRs include all primary containment space, although it may sometimes be appropriate to use only wetwell airspace, depending on sequence considerations. Partition coefficients were calculated as functions of temperature from Equation 27. The total iodine inventory initially deposited in water as I^- was calculated using previously mentioned mass inventories and release fractions and assuming a molecular weight of 130.

These various data and the quantities calculated from them are listed for each accident sequence in Table 3.5. From the table, it appears that PWRs exhibit dose rates considerably higher than do BWRs, contributing to the much higher conversion fractions. The presence of extremely large water volumes is a distinct advantage for BWRs in this regard. The conversion data of Lin[23] were taken at a dose rate of 4.5 Mrad/h in the range of PWR rates. The data taken at ORNL are generally in the range of BWR dose rates (i.e., 0.35 to 0.6 Mrad/h). Both sets of data indicate that conversion is dominated by pH effects. In this study, two scenarios were evaluated: (1) control of pH above 7 and (2) uncontrolled pH with resulting drops below 7 due to nitric acid. For

Table 3.5 Data for equilibrium analysis of example sequences

Plant	Accident	Volume (m^3)		Temperature (°C)	Partition coefficient	$\dot{E}_{dep}$ (MeV/h)* $\times 10^{-23}$	Dose rate** (Mrad/h)	Total I (g-mol)	Aqueous I_2 (%)†	
		Liquid	Gas						$\Delta t = 10$ h	$\Delta t = 15$ h
Grand	TCγ	4550	39650	102	5.0	1.2778	0.45	122.5	14	18
Gulf	TQUVγ	5171	39650	60	21.2	1.3020	0.40	136.2	13	18
Peach	AEγ	4000	7873	54	26.0	1.2223	0.49	127.7	16	21
Bottom	TC2	4500	7873	118	2.9	1.1997	0.43	114.9	14	19
Sequoyah	TBA	1465	36404	112	3.6	0.9267	1.01	105.2	24	30
Surry	TMLB′	115	51000	93	6.8	0.5136	7.16	57.2	59	67
	AB	172	51000	112	3.6	0.6912	6.44	85.8	58	66

*Calculated from Equation 23.
**Calculated from the expression: dose rate (Mrad/h) = $1.60219 \times 10^{-20} \dot{E}_{dep}/(\rho V_L)$, where $\rho = 1$ kg/L is assumed.
†Calculated from Equation 19.

this calculation, it was not necessary to specify the material that was used to control the pH at 7 or above.

If the pH is controlled so that it stays above 7, a reasonable value for the fraction of I^- converted to I_2 is 3×10^{-4} (Section 3.3.1.1). Using this and the other computed quantities in Table 3.5, the system of equations 32 is solved to yield the species distributions in Table 3.6. It should be noted that data in Tables 3.5 and 3.6 refer to the total iodine in containment, not the core inventory of iodine. Table 3.6 indicates a small production of volatiles for PWRs but virtually none for BWRs.

Such results are strongly dependent on the aqueous conversion fraction of $F = 3 \times 10^{-4}$, which represents a best estimate of the maximum from ORNL data. Thus, if pH is maintained at 7 or above, only a small additional amount of I_2 is expected in the gas phase in PWR systems.

If the pH falls below 7, a system for conrolling pH is not being used and the decreased pH results in a larger fraction of aqueous I^- being converted to I_2. Evaporation of this volatile species so as to maintain equilibrium partitioning will result in greater atmospheric I_2. This, in turn, yields higher organic iodide concentrations. The aqueous conversion fraction itself is determined from Equation 25, which requires a value for the equilibration time Δt. As discussed in Section 3.3.1, a value of $\Delta t = 15$ h is appropriate and yields the results shown in Table 3.7 for the equilibrium species distributions. As expected, the levels of airborne volatiles are much higher than in the controlled case, indicating almost complete conversion for PWRs.

The gaseous I_2 fraction is considerably higher in PWRs than in BWRs because the large water volumes in the latter both lower the dose rate and retain greater quantities of dissolved I_2. This last effect also depends on the gas volume and the ratio of gas to liquid volumes. It is ironic that the relatively small gas space in the Peach Bottom reactor (generally a safety liability) permits noticeably less evaporation than other reactors, resulting in the lowest gaseous I_2 fractions.

The other principal effect is due to temperature — the I_2 partition coefficient changes markedly over the range of temperatures used. This is most noticeable in the BWR sequences where different sequences at the same plant show large differences in the airborne I_2 fraction. Thus, an increase in containment temperature (at the gas-liquid interface) from 60 to 115°C (140 to 239°F) produces nearly an order of magnitude increase in the airborne fraction.

The organic iodide is present in PWRs at about 0.5% of core inventory; in BWRs, this concentration is closer to 0.1%. The I_2 generated by the radiolytic conversion of I^- dominates the amount released as I_2 from the RCS. Further, based on the equilibrium assumption, the presence of some I_2 already airborne will result in less evaporation of I_2 formed radiolytically. Hence, for the case of uncontrolled pH, the cumulative total is well represented by the equilibrium amount formed within containment.

3.3.3 Evaporation to Dryness

Water pools or condensate puddles may evaporate in containment and provide a mechanism for the release of dissolved aqueous iodine to the gas. As with all processes involving aqueous iodine, the extent of volatile iodine produced is related to pH. Table 3.8 gives percentages of volatile iodine produced when 1×10^{-4} mol/L CsI solutions were evaporated to dryness at 95°C. Radiation increased the percentage of volatile iodine by about an order of magnitude. In solutions where the initial pH was 7 or below, there was a rapid decrease in pH just before dryness.

The overall impact of evaporation to dryness will depend on the extent to which it occurs in containment.

Table 3.6 Distribution of iodine species for pH controlled above 7

Plant	Accident	Fraction of total iodine in containment (%)			
		I_2 (g)	I_2 (ℓ)	I^- (ℓ)	CH_3I (g)
Grand Gulf	TC γ	0.05	0.03	99.92	0.001
	TQUV γ	0.01	0.03	99.96	0.0003
Peach Bottom	AE γ	0.002	0.03	99.97	0.0001
	TC2 γ	0.02	0.03	99.95	0.0004
Sequoyah	TBA	0.21	0.03	99.76	0.004
Surry	TMLB′ γ	1.9	0.03	98.0	0.03
	AB γ	2.4	0.03	97.5	0.03

Table 3.7 Distribution of iodine species for uncontrolled pH

Plant	Accident	Fraction of total iodine in containment (%)			
		I_2 (g)	I_2 (ℓ)	I^- (ℓ)	CH_3I (g)
Grand Gulf	TC γ	26.6	15.3	58.0	0.2
	TQUV γ	6.6	18.3	75.1	0.06
Peach Bottom	AE γ	1.6	21.6	76.8	0.01
	TC2 γ	10.9	18.0	71.0	0.07
Sequoyah	TBA	69.2	9.9	20.5	0.4
Surry	TMLB′ γ	97.1	1.5	0.7	0.7
	AB γ	97.6	1.2	0.6	0.6

Table 3.8 Iodine volatility of 1×10^{-4} mol/L CsI solutions during evaporation to dryness

Test conditions		Percent volatile		
Initial pH	Borate (*M*)	Without radiation	With radiation (total dose, 2.1 MR)	Final pH just before dryness
4.4	0.2	7.2	>99	1.8 to 2.0
4.4	0*	2.0		3.6
6.0	0.2	6.8	55	2.0 to 2.2
7.0	0.2		32	3.0
Pure water	0	1.6	21	
9.0	0.2	1.8	22	8.5

*Phosphoric acid added to adjust the pH to 4.4.

4 Technical Findings

4.1 Perspective and Scope of Study

This study assumed that iodine forms in containment can be delimited by an examination of the seven severe accident sequences in LWR plants, along with an evaluation of associated processes. The associated processes include the deposition of CsOH on RCS surfaces and the effects of radiolysis. The issue is the chemical form of iodine that may be produced in the RCS and in containment — not the ultimate disposition of the various chemical forms. For example, it is likely that much of the gaseous I_2 in containment would be removed by engineered safety features or would deposit on painted or metal surfaces.

4.2 Assessment of Iodine Chemical Forms in the RCS

The maximum iodine as I plus HI calculated for the seven severe accident sequences is 3.2%. Iodine in all forms other than I, HI, and CsI is estimated to be less than 1%. Although this analysis only considered seven sequences at four plants, it is reasonable to consider that a maximum of 5% of the iodine would be present as elemental iodine and HI for all accident sequences. A minimum value would not be expected to be less than 1%. The remaining 95% of the iodine would be as CsI.

The gaseous forms of iodine that entered containment from the RCS were given in terms of both elemental iodine and HI. There is a fundamental reason for this. The two forms of iodine are related by

$$I + \frac{1}{2}H_2 \rightleftharpoons HI \qquad (37)$$

In the temperature range of 1000 to 2000 K, thermochemical data for this reaction were fit to give

$$\frac{P_{HI}}{P_I} = (P_{H_2})^{-1/2} \cdot \exp\left(\frac{1.024 \times 10^4}{T} - 5.645\right) \qquad (38)$$

Lower temperatures and higher hydrogen pressures tend to favor HI over I, with the opposite conditions favoring I over HI. Five percent of iodine as I plus HI, with not less than 1% in either form, means that the P_{HI}-to-P_I ratio in Equation 38 would range from 0.25 to 4. With a hydrogen pressure of 1 atm, this would occur in the temperature range of 1456 to 2404 K (2161 to 3868°F); with a hydrogen pressure of 10 atm, it would occur in the temperature range of 1251 to 1893 K (1792 to 2948°F). These conditions are reasonable for situations that lead to the formation of I or HI.

The major uncertainty is the extent to which CsOH will react with oxide materials and reduce its vapor pressure. If the reaction of CsOH is to have a major impact on the iodine chemical forms, most of it (certainly more than 90%) must be fixed at a very low vapor pressure.

4.3 Assessment of Iodine Chemical Forms in Containment

The production of I_2 in containment will be directly related to the pH levels of the water pools. As illustrated in Figure 4.1, failure to control the pH at or above 7 could result in an increase of I_2 in the atmosphere of between 4,100 and 33,000% as compared with the case where pH is controlled for PWRs. Essentially all of the I_2 could become gaseous in the PWRs without pH control. For BWRs, the increase is between 53,000 and 80,000%, with about 25% of the I_2 becoming gaseous. The dramatic difference in the amount of I_2 between the cases where pH was uncontrolled below 7 and the controlled cases speak for themselves. A major uncertainty is the extent of evaporation to dryness. From 2 to 20% of the iodine in water pools that have evaporated could be converted to a volatile form, most likely as I_2.

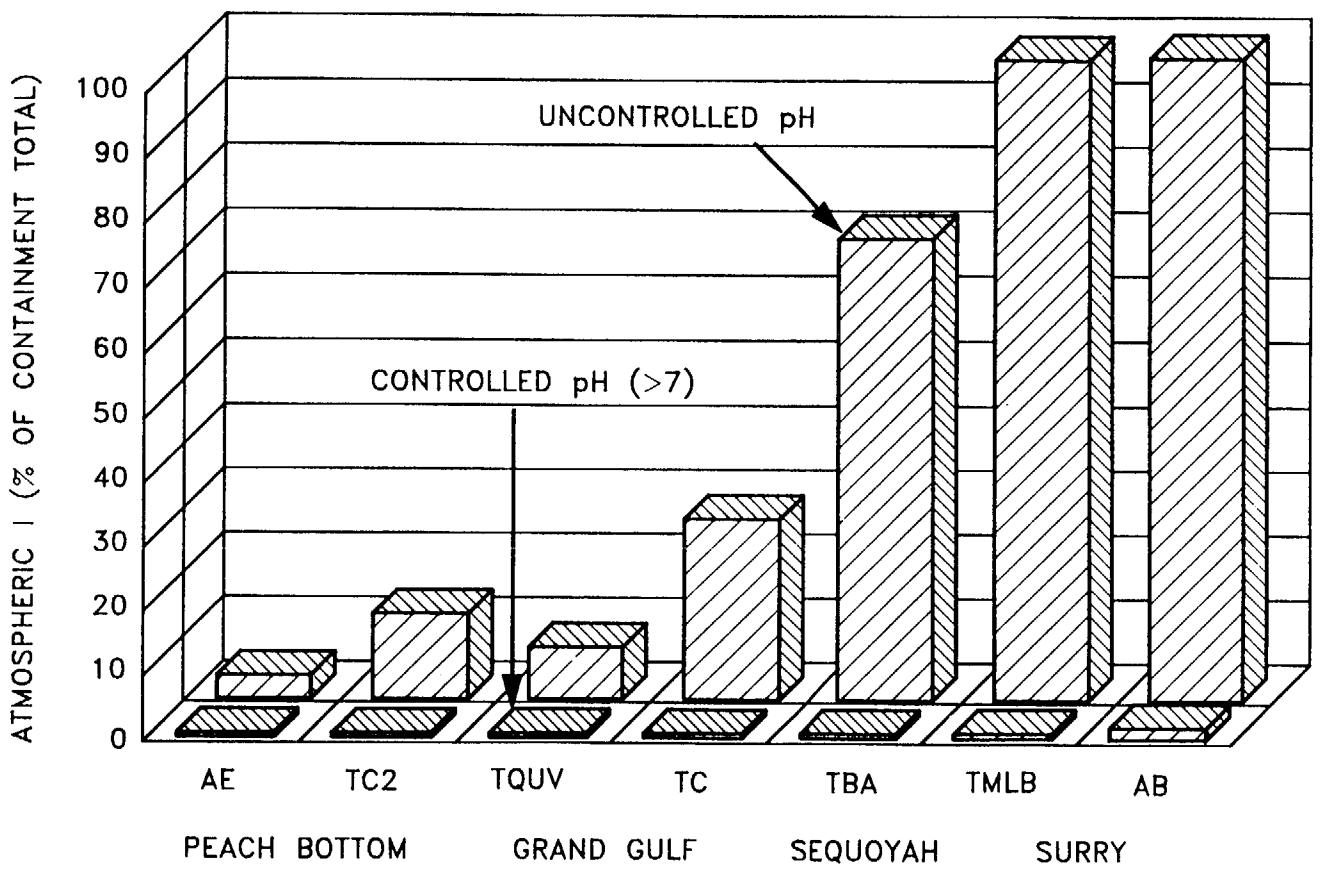

Figure 4.1 Additional atmospheric elemental iodine released

5 References

1. Gieseke, J. A. et al., "Radionuclide Release Under Specific LWR Accident Conditions," BMI-2104, Battelle Columbus Laboratories, 1984.

2. Denning, R. S. et al., "Radionuclide Release Calculations for Selected Severe Accident Scenarios," NUREG/CR-4624 (BMI-2139), Battelle Columbus Laboratories, 1986.

3. FACT, a copyrighted product of THERMFACT Ltd., 447 Berwich Ave., Mount-Royal, Quebec, Canada, H3R 1Z8.

4. Wisby, S. J. et al., "Iodine Behavior in Containment Under LWR Accident Conditions," pp. 6–29 in *Proceedings of the Symposium on Chemical Phenomena Associated with Radioactivity Releases During Severe Nuclear Plant Accidents*, Anaheim, Calif., September 1986.

5. Beahm, E. C., W. E. Shockley, and O. L. Culberson, "Organic Iodide Formation Following Nuclear Reactor Accidents," NUREG/CR-4327, Oak Ridge National Laboratory, 1985.

6. Lemire, R. J. et al. "Assessment of Iodine Behavior in Reactor Containment Buildings from a Chemical Perspective," AECL-6812, 1981.

7. Burns, W. G. et al., "The Radiolysis of Aqueous Solutions of Caesium Iodide and Caesium Iodate," AERE-R-13520, 1990.

8. U.S. Nuclear Regulatory Commission, Regulatory Guide 1.3, "Assumptions Used for Evaluating the Potential Radiological Consequences of a Loss-of-Coolant Accident for Boiling Water Reactors," June 1974.

9. U.S. Nuclear Regulatory Commission, Regulation Guide 1.4, "Assumptions Used for Evaluating the Potential Radiological Consequences of a Loss-of-Coolant Accident for Pressurized Water Reactors," June 1974.

10. Wooten, R. O., P. Cybulskis, and S. F. Quayle, "MARCH2 Meltdown Accident Response Characteristic Code Description and User's Manual," NUREG/CR-3988 (BMI-2115), Battelle Columbus Laboratories, 1984.

11. Jordan, H. and M. R. Kuhlman, "TRAP-MELT User's Manual," NUREG/CR-4205 (BMI-2124), Battelle Columbus Laboratories, 1985.

12. Chance, E. M. et al., "FACSIMILE: A Computer Program for Flow and Chemistry Simulation, and General Initial Value Problems," AERE-R-8775, AERE Harwell, December 1977.

13. Johnson, I. et al., "Downstream Behavior of Volatile Iodine, Cesium, and Tellurium Fission Products," EPRI NP-6182, January 1989.

14. Silberberg, M. et al., "Reassessment of Technical Bases for Estimating Source Terms," NUREG-0956, U.S. Nuclear Regulatory Commission, July 1986.

15. Megaw, W. J. and F. G. May, "The Behavior of Iodine Released in Reactor Containers," *J. Nucl. Energy, Pts. A/B*, **16**, 427 (1962).

16. Croft, J. F. and R. S. Isles, "Experimental Release of Radioiodine in the Zenith Reactor Containment," AEEW-R-172, 1962.

17. Parker, G. W., G. E. Creek, and W. J. Martin, "Fission Product Transport and Behavior in the Stainless Steel-Lined Containment Research Installation," ORNL-4502, 1971.

18. Hilliard, R. K. and L. F. Coleman, "Natural Transport Effects on Fission Product Behavior in the Containment Systems Experiment," BNWL-1457, 1970.

References

19. Cline, J. E. et al., "Measurements of ^{129}I and Radioactive Particulate Concentrations in the TMI-2 Containment Atmosphere During and After the Venting," GEND-009, April 1981.

20. Lillian, D. et al., *Environ. Sci. Technol.* **12**, 1042 (1975).

21. Bates, R. G., *Determination of pH*, p. 99, Wiley, New York, 1964.

22. Beahm, E. C. and W. E. Shockley, "Method for Gettering Organic, Inorganic, and Elemental Iodine in Aqueous Solutions," Patent ESID 518-X (April 1989).

23. Lin, C. C., "Chemical Effects of Gamma Radiation on Iodine in Aqueous Solutions," *J. Inorg. Nucl. Chem.* **42**, 1101 (1980).

24. Naritami, M. et al., "Batch-Type Tests on Formation of Volatile Iodine Species from Aqueous Iodide Solutions Under ^{60}Co γ-Ray Irradiation," *Proceedings of the Third CSNI Workshop on Iodine Chemistry in Reactor Safety*, Sept. 11-13, 1991, Toaki-mura, Japan.

25. Croff, A. G., "ORIGEN2 — A Revised and Updated Version of the Oak Ridge Isotope Generation and Depletion Code," ORNL-5621, Oak Ridge National Laboratory, July 1980.

26. Weber, C. F., "Calculation of Absorbed Doses to Water Pools in Severe Accident Sequences," ORNL/CSD/TM-274, Oak Ridge National Laboratory, 1991.

27. Nourbakhsh, H. P., "Estimate of Radionuclide Release Characteristics into Containment Under Severe Accident Conditions (Draft for Comment)," NUREG/CR-5747, Brookhaven National Laboratory, December 1991.

28. Eguchi, W., M. Adachi, and M. Yoneda, *J. Chem. Eng. Jpn.* **6**, 389 (1973).

29. Sanemasa, I. et al., *Bull. Chem. Soc. Jpn.* **57**, 1352 (1984).

30. Furrer, M., R. C. Cripps, and R. Gubler, *Nucl. Technol.* **70**, 290 (1985).

31. Postma, A. K. and R. V. Zavodoski, "Review of Organic Iodide Formation Under Accident Conditions in Water-Cooled Reactors," WASH-1233, U.S. Atomic Energy Commission, 1972.

32. Wren, D. J., "Kinetics of Iodine and Cesium Reactions in the CANDU Reactor Primary Heat Transport System Under Accident Conditions," AECL-7781, April 1983.

33. Frost, A. and B. Pearson, **Kinetics and Mechanism**, 2nd ed., p. 104, Wiley, New York, 1961.

34. Lorenz, K., H. Wagner, and R. Zellner, *Ber. Buns. Phys. Chem.* **83**, 556 (1979).

35. Kondrat'ev, V., *Kinetics of Chemical Gas Reactions*, AEC-tr-4493, 1958.

36. Chase, M. W., Jr. et al., *JANAF Thermochemical Tables*, 3rd ed., American Chemical Society, Washington, D.C., 1986.

37. Barin, I. and O. Knacke, *Thermochemical Properties of Inorganic Substances*, Springer-Verlag, Berlin, 1973.

Appendix A. Data from Accident Sequence Calculations

Table A.1 Grand Gulf TC–MERGE output data from MARCH2

Time (s)	Flow rate from core (lb/s)		Core exit temperature (°F)	Pressure (psia)
	Hydrogen	Total		
5381	0.0	0.543E+03	363	146
5498	0.0	0.591E+02	565	117
5504	0.319E-06	0.560E+02	578	117
5522	0.109E-05	0.480E+02	600	116
5552	0.656E-05	0.394E+02	641	115
5588	0.399E-04	0.333E+02	685	113
5612	0.112E-03	0.301E+02	710	112
5642	0.348E-03	0.270E+02	738	111
5678	0.110E-02	0.242E+02	768	110
5726	0.370E-02	0.208E+02	803	109
5756	0.669E-02	0.193E+02	825	108
5822	0.177E-01	0.138E+02	849	106
5858	0.181E-01	0.115E+02	851	105
5924	0.212E-01	0.996E+01	867	103
5978	0.251E-01	0.936E+01	884	102
6032	0.303E-01	0.884E+01	902	101
6080	0.360E-01	0.841E+01	920	100
6122	0.420E-01	0.822E+01	934	99
6182	0.525E-01	0.762E+01	963	98
6218	0.601E-01	0.724E+01	978	97
6284	0.772E-01	0.643E+01	1004	96
6326	0.901E-01	0.611E+01	1021	95
6380	0.110E+00	0.579E+01	1042	94
6446	0.139E+00	0.527E+01	1069	93
6512	0.172E+00	0.472E+01	1094	92
6578	0.212E+00	0.412E+01	1120	91
6647	0.251E+00	0.410E+01	1144	90
6691	0.270E+00	0.361E+01	1159	89
6742	0.301E+00	0.310E+01	1176	89
6836	0.302E+00	0.190E+01	1206	87
6911	0.308E+00	0.162E+01	1231	87
6974	0.320E+00	0.135E+01	1252	86
7075	0.308E+00	0.119E+01	1283	85
7126	0.300E+00	0.113E+01	1298	84
7176	0.294E+00	0.107E+01	1313	84
7252	0.286E+00	0.983E+00	1334	83
7327	0.280E+00	0.886E+00	1355	82
7390	0.274E+00	0.809E+00	1374	82
7478	0.269E+00	0.692E+00	1402	81
7617	0.257E+00	0.569E+00	1444	80

Table A.1 (Continued)

Time (s)	Flow rate from core (lb/s)		Core exit temperature (°F)	Pressure (psia)
	Hydrogen	Total		
7705	0.245E+00	0.539E+00	1469	79
7831	0.230E+00	0.502E+00	1504	78
7995	0.218E+00	0.467E+00	1550	77
8159	0.206E+00	0.431E+00	1595	76
8260	0.199E+00	0.408E+00	1622	75
8398	0.190E+00	0.377E+00	1657	75
8474	0.180E+00	0.347E+00	1676	74
8600	0.168E+00	0.302E+00	1703	74
8688	0.160E+00	0.270E+00	1720	73
8827	0.149E+00	0.218E+00	1745	73
9129	0.127E+00	0.127E+00	1823	72
9356	0.108E+00	0.108E+00	1874	71
9734	0.920E-01	0.920E-01	1953	70
10409	0.578E-01	0.578E-01	2079	70
10484	0.639E-01	0.639E-01	2094	70
10514	0.525E+01	0.989E+01	2216	70
10559	0.796E+00	0.796E+00	2286	70
10574	0.0	0.0	721	70
10769	0.0	0.0	727	70
10784	0.206E+01	0.206E+01	2306	70
10814	0.436E+01	0.745E+01	2347	70
10874	0.480E+01	0.958E+01	2588	71
10904	0.107E+02	0.166E+02	2874	125
10915	0.176E+02	0.278E+02	306	119
10924	0.0	0.513E+01	308	113
10931	0.0	0.0	891	107
10962	0.0	0.0	891	83
10969	0.0	0.837E+02	315	79
10975	0.0	0.201E+03	312	75
10987	0.0	0.219E+03	304	72
11000	0.0	0.318E+02	304	72
11027	0.0	0.420E+02	305	72
11871	0.0	0.468E+02	303	70
13251	0.0	0.470E+02	303	71
13257	0.0	0.318E+03	309	70
13277	0.0	0.453E+02	303	71
15067	0.0	0.481E+02	303	70
15095	0.0	0.181E+01	302	70
15115	0.0	0.0	345	70
15410	0.0	0.0	345	70

Table A.2 Grand Gulf TC–MARCH2 output for input to TRAP-MELT

Time (s)	Flows from core (g/s)	
	CsI	CsOH
0	41.5	414
96	9.81	59.3
276	11.7	70.6
444	12.3	74.6
612	11.8	73.9
780	12.0	72.5
960	11.0	66.5
1150	10.4	62.7
1340	9.69	58.6
1550	8.57	51.8
1780	8.08	48.9
2070	7.10	43.0
2440	6.17	37.3
2810	5.70	34.5
3111	12.5	75.6
3290	15.9	96.0
3490	7.06	42.7
3760	0.98	5.93
4020	0.27	1.63
5350	0.08	0.5

Table A.3 Grand Gulf TC—MARCH2 output for input to TRAP-MELT

Time (s)	Pressure (psia)	Average gas temperature (°F)			
		Volume 1	Volume 2	Volume 3	Volume 4
0	1370	640	597	590	582
135	1420	640	597	590	582
405	1520	640	597	590	582
675	1620	651	603	590	582
945	1720	651	603	590	582
1230	1830	651	603	590	582
1530	1930	661	608	590	582
1830	2030	661	608	590	582
2160	2120	661	608	590	582
2490	2210	669	612	590	582
2810	2300	679	615	583	585
3100	2960	1040	730	768	664
3360	1740	1830	1420	1420	1170
3630	568	1290	1420	1120	1240
3930	567	860	1080	836	1040
4250	567	686	812	697	832
4580	603	669	764	668	800
4890	613	675	755	667	805
5400	613	675	755	667	805

Table A.4 Grand Gulf TQUV–MERGE output from MARCH2

Time* (s)	Flow rate from core (lb/s)		Core exit temperature (°F)
	H_2	Total	
0	0.0441	11.6	1255
120	0.0661	9.95	1315
180	0.0799	9.26	1346
300	0.114	8.30	1411
360	0.136	7.79	1444
420	0.162	7.01	1476
480	0.156	131	1765
543	0.132	110	1848
605	0.118	93.8	1902
664	0.109	83.5	1945
725	0.104	76.1	1980
843	0.103	62.5	2047
901	0.0966	58.4	20731
1087	0.0750	44.7	2123
1200	0.0703	37.2	2148
1260	0.0701	34.4	2159
1382	0.0748	28.8	2190
1566	0.0957	22.9	2250
1622	0.109	21.5	2272
1809	0.225	16.0	2413
1874	0.285	15.0	2514
2222	0.756	7.73	2794
2281	0.812	6.70	2846
2642	0.863	3.30	3053
2704	0.0	0.0	0
3020	0.647	1.42	3064
3064	0.604	1.31	3072
3346	0.638	1.20	3150
3603	0.506	0.719	3197
3661	0.296	0.377	3202
3904	0.0802	0.0802	3219
3969	0.0	0.0	0
4287	0.0547	0.0547	3135
4335	0.0127	0.0127	3130
4550	0.0	7.5	3120
4910	0.0	24.7	3100
5280	0.0	67.8	2980
5650	0.0	79.0	2920

Table A.4 (Continued)

Time* (s)	Flow rate from core (lb/s)		Core exit temperature (°F)
	H_2	Total	
6010	0.0	47.3	2800
6350	0.0	10.3	2740
6720	0.0	3.0	2650
6843	0.0	1.4	2604
7090	0.0	0.95	500
7440	0.0	0.49	500

*Note: All entries after t = 4335 are from TRAP-MELT input, with H_2 = 0 assumed, and most temperatures assumed (exception is point at t = 6843).

Table A.5 Grand Gulf TQUV—MARCH2 output for input to TRAP-MELT

Time (s)	Flows from core (g/s)	
	CsI	CsOH
0	36.1	337
130	8.76	54.1
325	15.5	93.2
451	17.6	106
577	18.1	110
704	17.8	108
886	10.3	64.2
1090	11.6	70.4
1230	16.1	97.6
1380	12.5	75.6
1590	10.5	63.3
1860	8.08	48.9
2670	4.67	28.2
3040	7.07	42.8
3340	6.85	41.4
3630	1.33	8.0
3940	0.35	2.1
4300	0.18	1.1
6840	0.03	0.21

Table A.6 Grand Gulf TQUV–MARCH2 output for input to TRAP-MELT

Time (s)	Pressure (psia)	Average gas temperature (°F)			
		Volume 1	Volume 2	Volume 3	Volume 4
0	100	2510	1690	1430	1050
204	81.9	2680	1730	1460	1050
619	56.4	2880	1800	1520	1040
1040	45.8	2970	1840	1550	914
1470	36.3	3150	1900	1580	1040
1890	32.4	3210	1940	1600	995
2300	31.0	3170	1948	1610	744
2690	78.2	3240	2090	1680	1300
3050	210	2670	2390	1920	1510
3420	327	422	2180	2150	1500
3790	345	431	1320	1740	1130
4150	261	407	936	1290	871
4490	84.6	321	931	1210	839
4860	39.0	268	935	1190	829
5230	31.0	253	937	1180	819
6300	26.0	240	938	1170	816
6900	25.0	240	938	1170	816

Table A.7 Peach Bottom AE–MERGE output for input to MARCH2

Time (s)	Flow rate from core (lb/s)		Core exit temperature (°F)
	H_2	Total	
0	0	0	1363
510	0.227	0.354	1363
690	0.219	0.337	1476
930	0.140	0.175	1568
1170	0.196	0.226	1746
1410	0.142	0.145	1865
1650	0.710	0.833	3141
1890	1.02	161	2610
2130	0.232	173	1178
2325	0.028	1.03	1606
2370	0	0	0
7000	0	0	0

Table A.8 Peach Bottom AE—MARCH2 output for input to TRAP-MELT

Time (s)	Flows from core (g/s)	
	CsI	CsOH
0	1.53	49.4
270	2.59	32.5
660	11.0	73.8
870	17.2	116
1050	18.5	124
1230	16.8	113
1410	14.8	99.6
1560	27.0	181
1680	28.9	194
1890	4.13	27.9
2340	1.92	12.9
3390	0.89	5.9
4500	1.56	10.5
5250	3.04	20.4
6300	1.47	9.9
6990	0.055	0.37

Table A.9 Peach Bottom AE–MARCH2 output for input to TRAP-MELT

Time (s)	Pressure (psia)	Average gas temperature (°F)		
		Volume 1	Volume 2	Volume 3
0	38.2	930	265	265
60	34.6	930	707	366
180	31.8	930	504	471
300	30.9	930	496	376
420	30.5	1220	517	398
600	30.5	1445	544	432
780	30.5	1550	554	430
960	30.5	1645	560	425
1140	30.5	1750	567	442
1260	30.5	1820	582	451
1380	30.6	1900	613	475
1500	34.2	2290	1040	954
1620	68.5	3210	1990	1900
1740	104	3250	2330	2220
1880	122	2340	2200	2120
2030	44	1270	1580	1550
2180	25.2	957	1270	1250
2300	15.4	1240	1340	775
2360	15.4	1240	1340	775
7000	15.4	1240	1340	775

Table A.10 Peach Bottom TC2—MERGE output from MARCH2

Time (s)	Flow rate from core (lb/s)		Core exit temperature (°F)	Pressure (psia)
	Hydrogen	Total		
3514	0.0	0.0	690	1105
3736	0.0	0.0	690	1104
3742	0.180E+00	0.544E+00	1690	1104
3778	0.257E+00	0.841E+00	1815	1108
3814	0.524E+00	0.188E+01	1843	1111
3850	0.174E+01	0.665E+01	1939	1124
3871	0.482E+01	0.255E+02	2059	1118
3881	0.680E+01	0.396E+02	2225	1109
3896	0.411E+01	0.189E+02	2149	1079
3913	0.0	0.0	736	1099
4066	0.0	0.0	736	1098
4072	0.116E+00	0.211E+00	2089	1098
4108	0.395E+00	0.117E+01	2180	1100
4144	0.142E+01	0.515E+01	2276	1111
4162	0.637E+00	0.206E+01	2258	1116
4174	0.0	0.0	765	1116
4186	0.277E+00	0.642E+00	2136	1117
4222	0.347E+00	0.854E+00	2257	1121
4258	0.391E+00	0.957E+00	2270	1125
4294	0.826E+00	0.250E+01	2294	1131
4301	0.414E+01	0.153E+02	2416	1099
4313	0.932E+01	0.167E+03	2940	1120
4328	0.916E+01	0.418E+02	2998	1101
4351	0.378E+01	0.141E+02	3031	1111
4356	0.0	0.0	883	1111
4523	0.0	0.0	883	1110
4529	0.418E+00	0.877E+00	2859	1110
4565	0.146E+01	0.406E+01	3061	1121
4601	0.120E+01	0.266E+01	3104	1132
4612	0.414E+01	0.134E+02	3146	1110
4622	0.826E+01	0.127E+03	3720	1120
4638	0.835E+01	0.375E+02	3748	1090
4657	0.475E+01	0.149E+02	3910	1123
4661	0.0	0.0	1063	1123
4701	0.0	0.0	1063	1120
4707	0.617E+00	0.132E+01	3651	1121
4743	0.174E+01	0.385E+01	3812	1138
4748	0.728E+01	0.231E+02	3800	1112
4759	0.716E+01	0.397E+02	3955	1122
4778	0.754E+01	0.391E+02	4079	1090

Table A.10 (Continued)

Time (s)	Flow rate from core (lb/s)		Core exit temperature (°F)	Pressure (psia)
	Hydrogen	Total		
4790	0.500E+01	0.124E+02	4120	1129
4794	0.0	0.0	1238	1129
4821	0.0	0.0	1238	1127
4827	0.564E+00	0.118E+01	3865	1128
4863	0.213E+01	0.470E+01	3983	1146
4869	0.787E+01	0.441E+02	3998	1124
4878	0.670E+01	0.328E+02	4053	1139
4890	0.0	0.0	2101	1119
4905	0.713E+01	0.124E+03	4004	1132
5028	0.131E+01	0.282E+01	3967	1150
5033	0.567E+01	0.171E+02	3970	1122
5041	0.645E+01	0.920E+02	4016	1141
5055	0.738E+01	0.608E+02	4014	1106
5071	0.408E+01	0.112E+02	4040	1135
5075	0.0	0.0	1644	1135
5106	0.0	0.0	1644	1133
5112	0.870E+00	0.184E+01	3868	1135
5142	0.150E+01	0.324E+01	3989	1150
5148	0.662E+01	0.232E+02	3985	1122
5156	0.650E+01	0.786E+02	4025	1150
5169	0.673E+01	0.300E+02	4028	1116
5186	0.776E+01	0.231E+02	3153	1135
5193	0.256E+02	0.548E+02	559	1166
5195	0.0	0.219E+02	560	1149
5209	0.0	0.303E+03	558	1122
5246	0.0	0.124E+03	563	1161
5673	0.0	0.466E+02	562	1154
5709	0.0	0.145E+03	563	1156
6904	0.0	0.246E+02	561	1138
7589	0.0	0.117E+02	564	1168

Table A.11 Peach Bottom TC2–MARCH2 output for input to TRAP-MELT

Time (s)	Flows from core (g/s)	
	CsI	CsOH
3500	0	0
3504	72.5	667.1
3548	24.6	163.4
3676	13.0	87.0
3833	15.0	100.7
3968	17.3	116.3
4132	10.7	72.3
4295	18.0	122.7
4425	15.9	108.5
4585	11.9	83.4
4735	18.0	126.4
4859	16.5	113.0
5027	10.3	70.9
5173	22.8	171.6
5248	31.2	227.7
5361	2.7	19.6
6516	0.11	0.83
7587	0.007	0.05

Table A.12 Peach Bottom TC2–MARCH2 output for input to TRAP-MELT

Time (s)	Pressure (psia)	Average gas temperature (°F)			
		Volume 1	Volume 2	Volume 3	Volume 4
3500	1290	1090	884	740	671
3700	1290	1090	884	740	671
3706	1290	1090	884	740	671
3913	1490	1190	921	779	697
4114	1470	1190	895	790	672
4315	1710	1540	1300	913	816
4523	1940	1600	1200	936	793
4725	2380	1830	1250	1020	802
4923	2490	2140	1470	1240	955
5130	2480	2210	1640	1340	978
5329	567	968	1260	1420	1290
5535	567	764	1060	1250	1200
5738	567	651	859	1040	1100
5938	567	607	741	887	986
6547	568	576	601	649	718
7360	569	591	607	615	703
7600	569	591	607	615	703

Table A.13 Sequoyah TB—MERGE output from MARCH2

Time (s)	Flow rate from core (lb/s)		Core exit temperature (°F)
	H_2	Total	
19356	0.112	12.6	2460
19656	0.607	4.44	2637
19956	0.627	2.23	3010
20256	0.730	0.812	3352
20556	0.687	0.728	3505
20856	0.825	0.900	3617
21162	1.525	2.02	3772
21366	0	75.85	3288
21426	0	115.2	3210
21498	0	123.7	3135
21558	0	124.7	3070
21636	0	142.6	2991
21720	0	128.3	2904
21804	0	128.3	2813
21894	0	126.8	2728
21954	0	130.85	2667
22014	0	131.75	2602
22086	0	111.7	2528
22176	0	106.1	2440
22260	0	118.4	2355
22338	0	117.6	2280
22416	0	100.65	2203

Table A.14 Sequoyah TB—MARCH2 output for input to TRAP-MELT

Time (s)	Flows from core (g/s)	
	CsI	CsOH
19400	0	0
19643	16.39	146.2
19748	10.00	64.3
19913	17.00	103.8
20033	20.0	114.9
20145	20.9	121.9
20250	22.0	128.0
20355	22.5	132.3
20460	21.6	127.3
20565	20.3	119.6
20685	16.5	98.2
20828	15.0	88.9
20985	12.9	78.1
21163	10.4	63.8
21307	20.4	133.1
21481	0.67	4.3
22012	0.045	0.28
22414	0.002	0.01

Table A.15 Sequoyah TB—MARCH2 output for input to TRAP-MELT

Time (s)	Pressure (psia)	Average gas temperature (°F)			
		Volume 1	Volume 2	Volume 3	Volume 4
19400	1223	1830	1100	1050	671
19782	1223	1830	1100	1050	671
19923	1254	1910	1120	1070	675
20063	1282	1990	1150	1090	680
20198	1305	2090	1170	1110	676
20337	1327	2150	1210	1140	679
20475	1345	2180	1240	1170	681
20614	1360	2220	1280	1200	685
20753	1370	2240	1310	1240	690
20891	1407	2280	1370	1310	694
21030	1485	2310	1430	1370	706
21167	1588	2360	1500	1440	714
21306	1911	605	1010	1040	730
21444	2102	613	758	779	727
21584	2043	611	667	680	721
22419	1999	608	619	620	664

Table A.16 Surry TMLB'—MERGE output from MARCH2

Time (s)	Flow rate from core (lb/s)		Core exit temperature (°F)	Pressure (psia)
	Hydrogen	Total		
0	0.000E+00	0.298E+04	580	2250
2640	0.000E+00	0.667E+02	564	1599
2670	0.000E+00	0.369E+02	564	1619
2820	0.000E+00	0.802E+01	573	1816
5835	0.000E+00	0.784E+02	660	2369
5850	0.668E-07	0.782E+02	660	2369
5955	0.567E-06	0.691E+02	669	2369
6060	0.246E-05	0.518E+02	703	2369
6135	0.779E-05	0.409E+02	746	2369
6195	0.236E-04	0.335E+02	766	2369
6270	0.963E-04	0.266E+02	836	2369
6330	0.288E-03	0.224E+02	889	2369
6345	0.378E-03	0.216E+02	900	2369
6390	0.840E-03	0.191E+02	935	2369
6405	0.109E-02	0.184E+02	945	2369
6495	0.436E-02	0.149E+02	1009	2368
6570	0.105E-01	0.129E+02	1063	2368
6645	0.207E-01	0.110E+02	1116	2368
6705	0.327E-01	0.997E+01	1162	2368
6810	0.668E-01	0.786E+01	1241	2367
6900	0.121E+00	0.665E+01	1315	2367
6975	0.205E+00	0.543E+01	1380	2367
7020	0.302E+00	0.420E+01	1413	2366
7050	0.461E+00	0.252E+01	1426	2366
7185	0.434E+00	0.140E+01	1527	2366
7335	0.330E+00	0.526E+00	1638	2366
7545	0.202E+00	0.202E+00	1745	2365
7965	0.876E-01	0.876E-01	1892	2364
8235	0.000E+00	0.000E+00	663	2363
8340	0.000E+00	0.000E+00	663	2343
8400	0.799E+00	0.829E+00	2059	2354
8595	0.159E+01	0.202E+01	2689	2363
8625	0.508E+01	0.206E+02	3413	2363
8685	0.387E+01	0.705E+02	3852	2366
8700	0.675E+00	0.106E+03	660	2366
8715	0.000E+00	0.107E+03	660	2367
9045	0.000E+00	0.000E+00	944	2370

Table A.17 Surry TMLB'—MARCH2 output for input to TRAP-MELT

Time (s)	Flows from core (g/s)	
	CsI	CsOH
0	40.5	368
60	25.8	130
150	32.3	163
240	26.2	132
360	20.8	105
480	16.1	80.9
630	13.3	66.8
810	11.4	57.3
1020	8.1	41.0
1320	6.1	30.6
1650	7.2	36.1
2070	1.7	8.3
2340	0.7	3.7

Table A.18 Surry TMLB'—MARCH2 output for input to TRAP-MELT

Time (s)	Pressure (psia)	Average gas temperature (°F)	
		Volume 1	Volume 2
0	2370	1470	862
45	2365	1500	866
143	2360	1560	873
248	2358	1640	878
368	2356	1690	881
488	2354	1740	883
645	2353	1800	888
833	2352	1850	891
1020	2351	900	891
1240	2350	788	887
1470	2340	1780	930
1570	2360	2240	1090
1680	2365	3090	1730
1770	2370	1230	1200
1900	2370	660	758
1980	2370	660	719
2010	2370	660	756
2340	2370	660	784

Table A.19 Surry AB—MARCH2 output for input to TRAP-MELT

Time (s)	Flow rate from core (lb/s)		Core exit temperature (°F)
	H_2	Total	
0	0	0	1228
246	0.392	0.392	1228
312	0.353	0.353	1280
576	0.270	0.270	1471
906	0.233	0.233	1701
1170	0	40.3	3688
1230	1.393	40.7	3661
1470	6.083	40.25	3571
2070	0	40.7	3731
2706	0	0	3500
5000	0	0	3500

Table A.20 Surry AB—MARCH2 output for input to TRAP-MELT

Time (s)	Flows from core (g/s)	
	CsI	CsOH
0	162	1100
36	35.1	178
96	37.6	190
156	34.0	172
228	29.0	146
300	26.7	135
384	22.9	115
480	19.7	99.3
588	16.5	83.3
720	13.3	66.9
900	8.68	43.8
1180	4.4	22.3
1450	1.1	5.3
1630	0.62	3.2
1880	0.35	1.8
2520	0.21	1.1
4030	0.04	0.22
5190	0	0

Table A.21 Surry AB—MARCH2 output for input to TRAP-MELT

Time (s)	Pressure (psia)	Average gas Temperature (°F)	
		Volume 1	Volume 2
0	35.6	1040	724
198	34.6	0	803
330	34.0	1300	863
462	34.0	1400	920
726	32.5	1580	1010
858	32.1	1670	1060
990	31.9	1920	1200
1120	33.6	1010	974
1250	34.5	258	517
1390	35.5	260	419
1520	36.8	262	374
1650	37.6	263	352
2040	39.6	266	327
2280	40.9	267	321
2340	41.1	257	323
5120	41.1	257	323

Table A.22 Grand Gulf—Compartment volumes for sequences TC and TQUV

Control volume	Volume (ft^3)	
	TC	TQUV
Core	1728	1728
Steam separators	3357	3357
Steam dryers	3335	3335
Upper annulus	2030	2030
Relief line	208	208

Table A.23 Peach Bottom—Compartment volumes for sequences TC and AE

TC		AE	
Control volume	Volume (ft^3)	Control volume	Volume (ft^3)
Core	1360	Core	1728
Shroud head	1170	Steam separator	580
Pipes and separators	582	Upper outer annulus	2030
Steam dryers	3000		
Upper outer annulus	1000		
Lower outer annulus	1000		
Steam lines	1080		
Relief lines	622		

Table A.24 Sequoyah—Compartment volumes for sequence TBA

Control volume	Volume (ft^3)
Core	1020
Grid plate	70.01
Guide tubes	85.70
Upper support plate	511
Core barrel	857

Table A.25 Surry—Compartment volumes for sequences AB and TMLB

AB		TMLB	
Control volume No.	Volume (ft^3)	Control volume No.	Volume (ft^3)
1	589	1	589
2	100	2	100
3	506	3	506
4	79	4	230
5	150	6	1301

Appendix B. Kinetic and Equilibrium Calculations

B.1 Kinetics of Cs-I-H_2-H_2O Reactions

Twenty reactions (ten reversible equations) were chosen to represent the kinetic behavior of cesium and iodine species. In a more comprehensive study of the rates of formation of CsOH and CsI under accident conditions, Wren used 152 reactions.[30] In that study, he concluded that in a CANDU reactor primary heat transport system under accident conditions, CsI and CsOH would form in $<10^{-2}$ s. In the present study, the kinetic calculations are used only as a guide in determining which control volumes reached equilibrium (i.e., those control volumes in which the residence times of cesium and iodine species were sufficiently long that the species concentrations did not vary with time).

The data on equilibrium thermodynamics are generally more reliable than data on rate constants. For this reason, equilibrium thermochemical calculations were performed in addition to the rate calculations.

The rate constants for the 20 reactions given in Table B.1 is the Arrhenius form

$$K = A \exp\left(-\frac{E_{act}}{RT}\right) \qquad \text{(B.1)}$$

where

K = rate constant,
A = preexponential or frequency factor,
E_{act} = activation energy.

The rate constant equation written in this way assumes that there is little or no temperature dependence of A or E_{act} over the temperature range of interest.

In reactions of the type C + D ⇌ E + F, the rate constants for the forward and reverse reactions can satisfy the requirements of the equilibrium constant. The requirements of the equilibrium constraint to maintain A and E_{act} independent of temperature can be obtained as described in the following manipulation. The standard free energy change can often be fitted over a temperature interval by the simple linear relation

$$\underset{rxn}{\Delta G_F^\circ} = a + bT \qquad \text{(B.2)}$$

where

$\underset{rxn}{\Delta G_F^\circ}$ = standard free energy change of reaction,
a, b = constants fit over the same temperature interval.

If we adopt this means of expressing $\underset{rxn}{\Delta G_F^\circ}$, then

$$\underset{rxn}{\Delta G_F^\circ} = a + bT = RT \ln K_{eq} = -RT \ln \frac{K_F}{K_R} \qquad \text{(B.3)}$$

where

K_{eq} = equilibrium constant,
K_F, K_R = rate constant for the forward and reverse reactions.

Equation B.3 can be rearranged as

$$K_F = \exp\left[-\left(\frac{a}{RT} + \frac{b}{R}\right)\right] \cdot K_R \qquad \text{(B.4)}$$

The rate constants for the forward and reverse reactions are expressed as

$$K_F = A \exp\left(-\frac{E_{act_F}}{RT}\right) \qquad \text{(B.5)}$$

$$K_R = A' \exp\left(-\frac{E_{act_R}}{RT}\right) \qquad \text{(B.6)}$$

Inserting Equations B.5 and B.6 into B.4 gives

$$A \exp\left(-\frac{E_{act_F}}{RT}\right) = \exp\left[-\left(\frac{a}{RT} + \frac{b}{R}\right)\right] \cdot A' \exp\left(-\frac{E_{act_R}}{RT}\right) \qquad \text{(B.7)}$$

or

Appendix B

Table B.1 Reaction rate constants

Reaction	Rate constant* at 1000 K (1341°F)	Frequency factor	References
1. $CsI + H_2O \rightarrow CsOH + HI$	2.12×10^{-23}	1.57×10^{-12}	
2. $CsOH + HI \rightarrow CsI + H_2O$	1.00×10^{-15}	1.00 × 10-11	32
3. $2HI \rightarrow I_2 + H_2$	2.42×10^{-20}	1.00×10^{-10}	33
4. $I_2 + H_2 \rightarrow 2HI$	3.01×10^{-19}	1.66×10^{-10}	33
5. $I + I + M \rightarrow I_2 + M$	1.15×10^{-33}	3.17×10^{-34}	
6. $M + I_2 \rightarrow I + I + M$	2.56×10^{-17}	3.14×10^{-10}	
7. $I + H_2 \rightarrow HI + H$	2.19×10^{-17}	2.64×10^{-10}	
8. $HI + H \rightarrow I + H_2$	5.54×10^{-11}	7.4×10^{-11}	
9. $HI + I \rightarrow H + I_2$	4.66×10^{-18}	3.59×10^{-10}	34
10. $H + I_2 \rightarrow HI + I$	6.0×10^{-10}	6.0×10^{-10}	34, 35
11. $H + H + M \rightarrow H_2 + M$	1.25×10^{-35}	2.31×10^{-33}	
12. $M + H_2 \rightarrow H + H + M$	1.9×10^{-29}	4.98×10^{-9}	
13. $Cs + I + M \rightarrow CsI + M$	3.7×10^{-33}	6.44×10^{-31}	
14. $M + CsI \rightarrow Cs + I + M$	1.6×10^{-22}	5.37×10^{-9}	
15. $Cs + HI \rightarrow CsI + H$	2.00×10^{-11}	2.00×10^{-11}	32, 35
16. $CsI + H \rightarrow Cs + HI$	2.53×10^{-13}	2.82×10^{-13}	
17. $Cs + H_2O \rightarrow CsOH + H$	1.70×10^{-16}	1.11×10^{-9}	
18. $CsOH + H \rightarrow Cs + H_2O$	1.00×10^{-10}	1.00×10^{-10}	32
19. $Cs + I_2 \rightarrow CsI + I$	8.81×10^{-10}	8.81×10^{-10}	32
20. $CsI + I \rightarrow Cs + I_2$	8.66×10^{-20}	7.43×10^{-12}	

*Units are s^{-1}, cm^3-$molecule^{-1}$ s^{-1}, and cm^6-$molecule^{-2}$ s^{-1} for first-, second-, and third-order reactions, respectively. M, the collision molecule, is the total of the H_2 and H_2O molecular concentrations (molecules/cm^3).

$$\ln A - \frac{E_{act_F}}{RT} = \ln A' - \left(\frac{a}{RT} + \frac{b}{R}\right) - \frac{E_{act_R}}{RT} \qquad \text{(B.8)}$$

then

$$\ln A - \ln A' = \frac{E_{act_F} - E_{act_R}}{RT} - \left(\frac{a}{RT} + \frac{b}{R}\right) \qquad \text{(B.9)}$$

Assuming that $\ln A - \ln A' = -b/R$, then Equation B.9 becomes

$$\ln A - \ln A' = -\frac{b}{R} = \frac{E_{act_F} - E_{act_R}}{RT} - \left(\frac{a}{RT} + \frac{b}{R}\right) \qquad \text{(B.10)}$$

which yields

$$E_{act_F} - E_{act_R} = a \qquad \text{(B.11)}$$

Thus, fitting the standard free energy change of reaction to a linear form with temperature and assuming the difference in the natural log of the frequency factor for the forward and reverse reactions is equal to $-b/R$, then rate constants can be expressed in the Arrhenius form and satisfy the equilibrium constraint. Standard free energies of reaction in the form of $\Delta G^\circ = a + bT$ are given in Table B.2. These data were obtained from the FACT system.[3] The FACSIMILE computer program was used to perform the rate calculations.

B.2 Equilibrium Calculations in the Cs-I-H_2-H_2O System

The species considered in the equilibrium calculations include (gases) H_2, H_2O, CsOH, CsI, Cs, H, HI, I, and I_2; and (liquids) CsI, CsOH, Cs, and I_2. The calculations were performed with the EQUILIB routine of the FACT system. This method of calculation was chosen because it is readily accessible to anyone in North America and because the thermochemical data base of FACT comes from standard assessed sources such as JANAF[36] and Barin and Knacke.[37] Thermochemical data for CsOH are not part of the FACT[3] data base, and values from JANAF were inserted into a user's data base for these calculations.

The 13 species used in the equilibrium calculations are the same as those used in the kinetic calculations. Iodine ratios such as HI/CsI are very similar in the equilibrium calculations and in the kinetic calculations, primarily because the bimolecular rate constants are consistent with the equilibrium constants.

Table B.2 Standard free energy of reaction 500 to 1200 K (441 to 1701°F) written as $\Delta G^\circ_{rxn_F} = a + bT$, exothermic reaction expressed left to right (Energy in joules)

Reaction	*a*	*b*
$CsOH + HI \rightleftharpoons CsI + H_2O$	-1.31368×10^5	-1.54100×10^1
$I_2 + H_2 \rightleftharpoons 2HI$	-1.30038×10^4	-1.48455×10^1
$HI + H \rightleftharpoons I + H_2$	-1.37991×10^5	$+1.05761 \times 10^1$
$H + I_2 \rightleftharpoons HI + I$	-1.50995×10^5	-4.26918×10^0
$Cs + HI \rightleftharpoons CsI + H$	-8.80264×10^2	-3.54386×10^1
$CsOH + H \rightleftharpoons Cs + H_2O$	-1.30488×10^5	$+2.00288 \times 10^1$
$Cs + I_2 \rightleftharpoons CsI + I$	-1.51875×10^5	-3.97080×10^1

Appendix C. Fitting of Radiolysis Data

Data from Lin[14] are listed in Table C.1 and shown in Figure C.1. The fraction of I^- converted by radiolysis to I_2 must satisfy

$$\lim_{pH \to \infty} F = 0 \qquad \lim_{pH \to -\infty} F = 1 \qquad \text{(C.1a,b)}$$

which are identical to the conditions

$$\lim_{pH \to \infty} \ln\left(\frac{1}{F} - 1\right) = \infty \qquad \lim_{pH \to -\infty} \ln\left(\frac{1}{F} - 1\right) = -\infty$$

As shown in Figure C.1, there is a highly linear relationship between $\ln(\frac{1}{F} - 1)$ and pH. Using the data in Table C.1, a linear least-squares fit of the form

$$\ln\left(\frac{1}{F} - 1\right) = \alpha \cdot pH + \beta$$

yielded the values $\alpha = 1.72$ and $\beta = -6.08$ with a correlation coefficient of 0.94.

Table C.1 Radiolysis data* for formation of I_2

Initial concentration (mol/L)	Initial pH	Conversion (%)
10^{-3}	2	88.2
	3	81.8
	4	8.6
	5	2.4
	6	2.4
10^{-4}	3	93.8
	5	8.0
	6.6	1.7
10^{-5}	2	89.1
	3	77.9
	4	44.4
	5	6.9
	6.3	0.3

*Taken from C. C. Lin.[14]

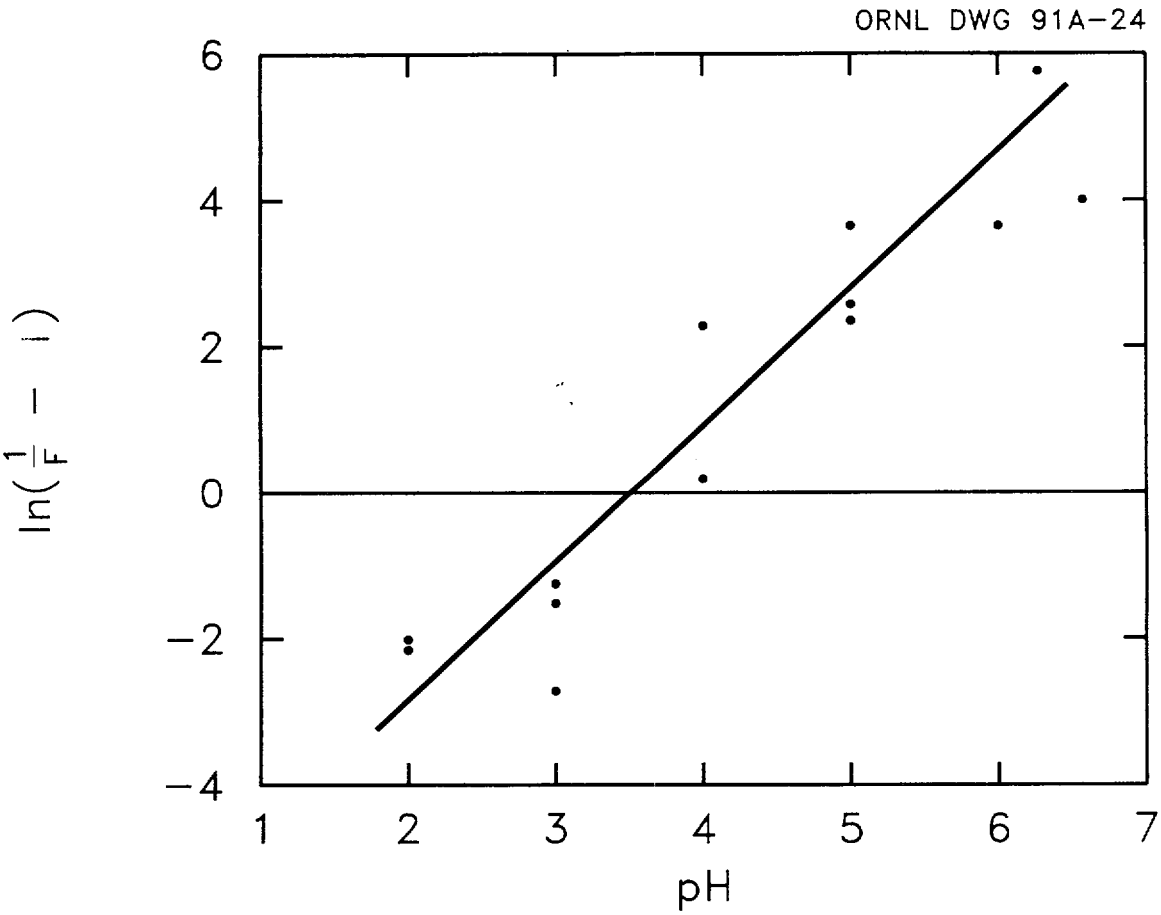

Figure C.1. Data fitting for radiolytic conversion of I^- to I_2 (data from U.S. Nuclear Regulatory Commission, Regulation Guide 1.4, "Assumptions Used for Evaluating the Potential Radiological Consequences of a Loss-of-Coolant Accident for Pressurized Water Reactors")

Appendix D. Fission Product Release Tables

Table D.1. Fission product inventories for selected plants*

Nuclide group		Total core inventory (kg)			
		Grand Gulf	Peach Bottom	Sequoyah	Surry
1	I	17.7	16.6	15.2	12.4
2	Cs	244.8	230.3	184.7	145.7
3	Te	37.1	34.9	31.7	25.4
4	Sr	66.7	62.7	60.9	47.6
5	Ba	112	105	77.7	61.2
6	Ru	621	584	470	369
7	Ce	221	208	167	131
8	La	1724	2404	1313	855
9	Xe	439	413	347	273

*Taken from References 1 and 2.

Table D.2. Bounding values for fractions of core inventory released into containment*

Fission product group	PWR releases into containment				BWR releases into containment			
	From primary system**		From core-concrete interaction		From primary system**		From core-concrete interaction	
	High RCS pressure	Low RCS pressure	Limestone concrete	Basaltic concrete	High RCS pressure	Low RCS pressure	Limestone concrete	Basaltic concrete
I	0.45	0.77	0.15	0.15	0.70	0.77	0.15	0.15
Cs	0.42	0.77	0.15	0.15	0.65	0.76	0.15	0.15
Te	0.27	0.51	0.40	0.30	0.17	0.17	0.50	0.30
Sr-Ba	0.013	0.01	0.40	0.15	0.013	0.01	0.70	0.30
Ru	0.053	0.01	0.005	0.005	0.053	0.01	0.005	0.005
La-Ce	0.01	0.0015	0.05	0.05	0.01	0.0015	0.10	0.10
Xe	1.0	1.0	0	0	1.0	1.0	0	0

*Adapted from H. P. Nourbakhsh, "Estimate of Radionuclide Release Characteristics Into Containment Under Severe Accident Conditions (Draft for Comment)" NUREG/CR-5747, Brookhaven National Laboratory, December 1991.

**Includes releases due to in-vessel melting, vessel breach, and late revaporization.

Appendix E. Fractional Release Tables

Table E.1 Grand Gulf — fractional releases and energy deposition rates

Nuclide group	Whole core inventory* (kg)	Total fraction released into containment**		Energy deposition rate, $\dot{E}_{dep}$ (MeV/h × 10^{-22})	
		Low RCS pressure	High RCS pressure	Low RCS pressure	High RCS pressure
I	17.7	0.92	0.85	6.921	6.394
Cs	244.8	0.91	0.80	0.885	0.778
Te	37.1	0.67	0.67	0.499	0.499
Sr	66.7	0.71	0.713	1.480	1.486
Ba	112	0.71	0.713	0.708	0.711
Ru	621	0.015	0.058	0.062	0.238
Ce	1055	0.1015	0.11	0.165	0.179
La	890	0.1015	0.11	2.300	2.493
Total				13.020	12.778

*From J. A. Gieseke et al., "Radionuclide Release Under Specific LWR Accident Conditions," BMI-2104, Battelle Columbus Laboratories, 1984, and R. S. Denning et al., "Radionuclide Release Calculations for Selected Severe Accident Scenarios," NUREG/CR-4624 (BMI-2139), Battelle Columbus Laboratories, 1986.

**Adapted from H. P. Nourbakhsh, "Estimate of Radionuclide Release Characteristics into Containment Under Severe Accident Conditions (Draft for Comment)," NUREG/CR-5747, Brookhaven National Laboratory, December 1991, assuming limestone concrete.

Table E.2 Peach Bottom — fractional releases and energy deposition rates

Nuclide group	Whole core inventory* (kg)	Total fraction released into containment**		Energy deposition rate, $\dot{E}_{dep}$ (MeV/h × 10^{-22})	
		Low RCS pressure	High RCS pressure	Low RCS pressure	High RCS pressure
I	16.6	0.92	0.85	6.491	5.997
Cs	230.3	0.91	0.80	0.833	0.732
Te	34.9	0.67	0.67	0.469	0.469
Sr	62.7	0.71	0.713	1.391	1.397
Ba	105	0.71	0.713	0.664	0.667
Ru	584	0.015	0.058	0.058	0.224
Ce	992	0.1015	0.11	0.155	0.168
La	836.6	0.1015	0.11	2.162	2.343
Total				12.223	11.997

*From J. A. Gieseke et al., "Radionuclide Release Under Specific LWR Accident Conditions," BMI-2104, Battelle Columbus Laboratories, 1984, and R. S. Denning et al., "Radionuclide Release Calculations for Selected Severe Accident Scenarios," NUREG/CR-4624 (BMI-2139), Battelle Columbus Laboratories, 1986.

**Adapted from H. P. Nourbakhsh, "Estimate of Radionuclide Release Characteristics into Containment Under Severe Accident Conditions (Draft for Comment)," NUREG/CR-5747, Brookhaven National Laboratory, December 1991, assuming limestone concrete.

Table E.3 Sequoyah — fractional releases and energy deposition rates

Nuclide group	Whole core inventory* (kg)	Total fraction released into containment**		Energy deposition rate, $\dot{E}_{dep}$ (MeV/h × 10^{-22})	
		Low RCS pressure	High RCS pressure	Low RCS pressure	High RCS pressure
I	15.2	0.92	0.60	5.943	3.876
Cs	184.7	0.91	0.57	0.675	0.418
Te	31.7	0.92	0.67	0.579	0.426
Sr	60.9	0.41	0.413	0.780	0.786
Ba	77.7	0.41	0.413	0.284	0.286
Ru	470	0.015	0.058	0.046	0.180
Ce	796	0.0515	0.06	0.063	0.074
La	684	0.0515	0.06	0.897	1.045
Total				9.267	7.091

*From J. A. Gieseke et al., "Radionuclide Release Under Specific LWR Accident Conditions," BMI-2104, Battelle Columbus Laboratories, 1984, and R. S. Denning et al., "Radionuclide Release Calculations for Selected Severe Accident Scenarios," NUREG/CR-4624 (BMI-2139), Battelle Columbus Laboratories, 1986.

**Adapted from H. P. Nourbakhsh, "Estimate of Radionuclide Release Characteristics into Containment Under Severe Accident Conditions (Draft for Comment)," NUREG/CR-5747, Brookhaven National Laboratory, December 1991, assuming limestone concrete.

Table E.4 Surry TMLB′ — fractional releases and energy deposition rates

Nuclide group	Whole core inventory* (kg)	Total fraction released into containment**		Energy deposition rate, $\dot{E}_{dep}$ (MeV/h × 10^{-22})	
		Low RCS pressure	High RCS pressure	Low RCS pressure	High RCS pressure
I	12.4	0.92	0.60	4.848	3.162
Cs	145.7	0.92	0.57	0.532	0.330
Te	25.4	0.81	0.57	0.413	0.290
Sr	47.6	0.16	0.163	0.238	0.242
Ba	61.2	0.16	0.163	0.087	0.089
Ru	369	0.015	0.058	0.037	0.142
Ce	626	0.0515	0.06	0.050	0.058
La	539	0.0515	0.06	0.707	0.823
Total				6.912	5.136

*From J. A. Gieseke et al., "Radionuclide Release Under Specific LWR Accident Conditions," BMI-2104, Battelle Columbus Laboratories, 1984, and R. S. Denning et al., "Radionuclide Release Calculations for Selected Severe Accident Scenarios," NUREG/CR-4624 (BMI-2139), Battelle Columbus Laboratories, 1986.

**Adapted from H. P. Nourbakhsh, "Estimate of Radionuclide Release Characteristics into Containment Under Severe Accident Conditions (Draft for Comment)," NUREG/CR-5747, Brookhaven National Laboratory, December 1991, assuming basaltic concrete.

NUREG/CR-5732
ORNL/TM-11861
Dist. Category R3

INTERNAL DISTRIBUTION

1. W. S. Aaron
2. C. W. Alexander
3. F. Barrera
4-8. E. C. Beahm
9. J. T. Bell
10. D. O. Campbell
11. J. L. Collins
12. W. Fulkerson
13. R. K. Genung
14. J. R. Hightower
15. E. K. Johnson
16. M. J. Kania
17-21. T. S. Kress
22. R. A. Lorenz
23. J. C. Mailen
24. M. F. Osborne
25-29. G. W. Parker
30. C. E. Pugh
31. M. G. Stewart
32. R. P. Taleyarkhan
33-37. C. F. Weber
38. Central Research Library
39. ORNL—Y-12 Technical Library Document Reference Section
40-41. Laboratory Records
42. Laboratory Records, ORNL RC
43. ORNL Patent Section

EXTERNAL DISTRIBUTION

44. Office of Assistant Manager for Energy Research and Development, DOE-OR, P.O. Box 2001, Oak Ridge, TN 37831
45. Director, Division of Reactor Safety Research, U.S. Nuclear Regulatory Commission, Washington, DC 20555
46-47. Office of Scientific and Technical Information, P.O. Box 2001, Oak Ridge, TN 37831
48. Division of Technical Information and Document Control, U.S. Nuclear Regulatory Commission, Washington, DC 20555
49. R. Y. Lee, Accident Evaluation Branch, U.S. Nuclear Regulatory Commission, NLN-353, Washington, DC 20555
50. R. O. Meyer, U.S. Nuclear Regulatory Commission, Nuclear Regulatory Research, NLS-007, Washington, DC 20555
51. F. Eltawila, Accident Evaluation Branch, U.S. Nuclear Regulatory Commission, NLN344, Washington, DC 20555
52. K. S. Norwood, 8 Appleford Drive, Abingdon, Oxon OX14, 2DA, United Kingdom
53. S. J. Wisbey, B.220, AERE Harwell, Didcot, Oxon OX11 ORA, United Kingdom
54. T. Yamashita, Nuclear Fuel Chemistry Laboratory, Department of Chemistry, Japan Atomic Energy Research Institute, Tokai-mura, Naka-gun, Ibaraki-ken, 319-11, Japan
55. S. Hagen, Bau 601, Kernforschungszentrum Karlsruhe, Postface 3640, D7500 Karlsruhe 1, Federal Republic of Germany
56. M. L. Brown, 15 Barrock St., Thurso Caithness, Scotland KW14 7DB
57. T. Nakamura, Reactivity Accident Laboratory, Dai-2-Genken-Shinhara-Jutaku-304, 1-23-5, Shinhara, Mito-shi, 310, Japan
58. H. K. Lee, Spent Fuel Storage and Disposal Technology Section, Korea Advanced Energy Research Institute, P.O. Office Box 7, Dae-Danji Choong-Nam, Republic of Korea
59. Y.-C. Tong, Institute of Nuclear Energy Research, P.O. Box 3-6, Lung-Tan, Taiwan, Republic of China
60. D. Williams, Technology Division, AEE Winfrith, Dorchester, Dorset, England
61. F. C. Inglesias, AECL, Chalk River Nuclear Laboratories, Chalk River, Ontario, KOJ 1JO, Canada
62. R. R. Hobbins, EG&G Idaho, Inc., P.O. Box 1625, Idaho Falls, ID 83401
63. D. A. Petti, EG&G Idaho, Inc., P.O. Box 1625, Idaho Falls, ID 83401

64. D. J. Osetek, Sandia National Laboratory, P.O. Box 5800, Albuquerque, NM 87185
65. K. O. Reil, Sandia National Laboratory, P.O. Box 5800, Albuquerque, NM 87185
66. D. Powers, Sandia National Laboratory, P.O. Box 5800, Albuquerque, NM 87185
67. L. A. Neimark, Argonne National Laboratory, 9700 South Cass Ave., Argonne, IL 60439
68. J. Rest, Argonne National Laboratory, 9700 South Cass Ave., Argonne, IL 60439
69. Y. Y. Liu, Argonne National Laboratory, 9700 South Cass Ave., Argonne, IL 60439
70. C. A. Alexander, Battelle Memorial Institute, 505 King Ave., Columbus, OH 43201
71. F. Panisko, Pacific Northwest Laboratory, P.O. Box 999, Richland, WA 99352
72. K. Y. Suh, Fauske & Associates, Inc., 16W070 West 83rd St., Burr Ridge, IL 60521

73-322. Given distribution as shown in Category R3 (NTIS - 10)

NRC FORM 335 (2-89) NRCM 1102, 3201, 3202

U.S. NUCLEAR REGULATORY COMMISSION

BIBLIOGRAPHIC DATA SHEET

(See instructions on the reverse)

1. REPORT NUMBER (Assigned by NRC, Add Vol., Supp., Rev., and Addendum Numbers, if any.)

NUREG/CR-5732
ORNL/TM-11861

2. TITLE AND SUBTITLE

Iodine Chemical Forms in LWR Severe Accidents

Final Report

3. DATE REPORT PUBLISHED

MONTH	YEAR
April	1992

4. FIN OR GRANT NUMBER

B0854

5. AUTHOR(S)

E. C. Beahm, C. F. Weber, T. S. Kress, and G. W. Parker

6. TYPE OF REPORT

Technical

7. PERIOD COVERED *(Inclusive Dates)*

8. PERFORMING ORGANIZATION – NAME AND ADDRESS *(If NRC, provide Division, Office or Region, U.S. Nuclear Regulatory Commission, and mailing address; if contractor, provide name and mailing address.)*

Oak Ridge National Laboratory
Oak Ridge, TN 37831-6285

9. SPONSORING ORGANIZATION – NAME AND ADDRESS *(If NRC, type "Same as above"; if contractor, provide NRC Division, Office or Region, U.S. Nuclear Regulatory Commission, and mailing address.)*

Division of Systems Research
Office of Nuclear Regulatory Research
U.S. Nuclear Regulatory Commission
Washington, DC 20555

10. SUPPLEMENTARY NOTES

11. ABSTRACT *(200 words or less)*

Calculated data from seven severe accident sequences in light water reactor plants were used to assess the chemical forms of iodine in containment. In most of the calculations for the seven sequences, iodine entering containment from the reactor coolant system was almost entirely in the form of CsI with very small contributions of I or HI. The largest fraction of iodine in forms other than CsI was a total of 3.2% as I plus HI. Within the containment, the CsI will deposit onto walls and other surfaces, as well as in water pools, largely in the form of iodide (I^-). The radiation-induced conversion of I^- in water pools into I_2 is strongly dependent on pH. In systems where the pH was controlled above 7, little additional elemental iodine would be produced in the containment atmosphere. When the pH falls below 7, however, it may be assumed that it is not being controlled and large fractions of iodine as I_2 within the containment atmosphere may be produced.

12. KEY WORDS/DESCRIPTORS *(List words or phrases that will assist researchers in locating the report.)*

iodine
fission product behavior
reactor containment
severe accidents
LWRs

13. AVAILABILITY STATEMENT

unlimited

14. SECURITY CLASSIFICATION

(This Page)

unclassified

(This Report)

unclassified

15. NUMBER OF PAGES

16. PRICE

THIS DOCUMENT WAS PRINTED USING RECYCLED PAPER